JOURNAL OF QUATERNARY SCIENCE (2024) **39**(4) 566–584 ISSN 0267-8179. DOI: 10.1002/jqs.3604

JQS Journal of Quaternary Science QRA Quaternary Research Association

# Refining Holocene sea-level variations for the Lofoten and Vesterålen archipelagos, northern Norway: implications for prehistoric human–environment interactions

**NICHOLAS L. BALASCIO,[1]* WILLIAM J. D'ANDREA,[2] ROGER C. CREEL,[2] LEAH MARSHALL,[1] MOUSSA DIA,[1] STEPHEN WICKLER,[3] R. SCOTT ANDERSON,[4] JACQUELINE AUSTERMANN,[2] KRISTIAN VASSKOG,[5] PÅL RINGKJØB NIELSEN[6] and SVEIN OLAF DAHL[5]**

[1]Department of Geology, William & Mary, Williamsburg, VA, USA
[2]Lamont-Doherty Earth Observatory of Columbia University, Palisades, NY, USA
[3]The Arctic University Museum of Norway, UiT The Arctic University of Norway, Tromsø, Norway
[4]School of Earth and Sustainability, Northern Arizona University, Flagstaff, AZ, USA
[5]Department of Geography, University of Bergen, Bergen, Norway
[6]Department of Earth Science, University of Bergen, Bergen, Norway

Received 1 September 2023; Revised 9 January 2024; Accepted 1 February 2024

ABSTRACT: The Lofoten and Vesterålen archipelagos are located off the outer coast of northern Norway far from the center of the former Fennoscandian Ice Sheet and near the continental shelf edge. Existing relative sea-level (RSL) data indicate a pronounced mid-Holocene transgression and interesting connections with the region's prehistoric human settlement history. Here we present seven new sea-level index points from isolation basins and five terrestrial limiting points from a coastal sedimentary sequence to refine the region's RSL history. Ingression and isolation contacts in isolation basin sediment cores are identified using sedimentary geochemical data, scanning X-ray fluorescence profiles and phytoplankton analysis. The ages of these contacts are determined using radiocarbon-based age models. Our index points range from 11.2 to 1.5k cal a BP and are combined with previously published data to predict the spatiotemporal evolution of sea level in this region using an ensemble of spatiotemporal empirical hierarchical models (STEHME). The new RSL curve constrains the timing of the mid-Holocene transgression, which occurred from c. 9 to 6k cal a BP when sea level increased from −4 to 7 m above present day. From c. 6 to 5k cal a BP, RSL rapidly fell to c. 4 m above present values, and more gradually declined at an average rate of c. 0.8 m $ka^{-1}$ over the last 5k cal a BP. Isobase maps derived using the STEHME show a decrease in the regional shoreline gradients since the transgression maximum from 0.25 to 0.07 m $km^{-1}$. Our data also better define how RSL variations influenced the location and preservation of coastal settlement locations and harbors from the early Stone Age through historic intervals, improving understanding of regional human–environment interactions.


KEYWORDS: Holocene; isolation basin; Lofoten; Norway; relative sea level; Vesterålen

## Introduction

Coastal Norway has experienced dramatic relative sea-level (RSL) variations since deglaciation driven primarily by global mean sea-level (GMSL) rise and vertical land movement due to glacial isostatic adjustment (GIA) (Creel et al., 2022). RSL changes are constrained by measurements of raised beaches, marine terraces, sedimentary sequences, isolation basins and archaeological sites. These reconstructions help test solid Earth models (Fjeldskaar, 1994; Steffen and Wu, 2011; Fjeldskaar and Bondevik, 2020), constrain ice loading history (Patton et al., 2017; Brendryen et al., 2020), and help understand spatial patterns in modern RSL and the potential risk that future RSL rise poses to coastal zones (Simpson et al., 2014).

Despite the wealth of postglacial sea-level data for Norway, the causes of RSL change at regional scales remain challenging to disentangle due to uncertainties in past ice sheet thickness, rates of melt and lateral variations in solid Earth properties. Improved field measurements are needed to fill spatial and temporal gaps in existing data, particularly in areas near the margins of the former Fennoscandian Ice Sheet (FIS) where the complex interplay between GIA and GMSL caused periods of alternating rise and fall in RSL. Detailed analyses of such regions offer insights into RSL and GIA processes at other former and extant marine-terminating ice margins, such as the Laurentide Ice Sheet (Barnhardt et al., 1995, 1997), the British–Irish Ice Sheet (Simms et al., 2022) and the West Antarctic Ice Sheet (Whitehouse et al., 2019). Moreover, RSL changes along the coast of Norway have played an important role in the regional early human history, influencing migration pathways, settlement locations and natural harbors, and guiding human–environment interactions (Glørstad, 2015).

RSL information can be obtained from a range of coastal environments that have defined relationships to former sea-level, i.e. *indicative meanings* (Shennan and Horton, 2002; Baranskaya et al., 2018; Creel et al., 2022). Data can be acquired as sea-level index points (SLIPs) whose indicative meanings relate them to a specific tidal datum, or as limiting points, which constrain RSL to above (marine limiting) or

*Correspondence: Nicholas L. Balascio, as above.
Email: nbalascio@wm.edu

below (terrestrial limiting) a geomorphic feature or sedimentary deposit (Shennan et al., 2015). Sea-level data for Norway produced in the mid- to late 20th century are primarily limiting points based on dates from raised beaches and marine terraces, which have considerable uncertainties in their vertical relationship to past sea level (Fægri 1944, Marthinussen 1962, Vorren 1978, Helskog 1978). More recently, SLIPs have been developed from coastal basins that became isolated from the ocean due to isostasy because these 'isolation basins' are ubiquitous in Norway and archive continuous sedimentary records that can be radiocarbon dated (e.g. Kjemperud, 1981; Svendsen and Mangerud, 1987, 1990; Corner and Haugane, 1993; Corner et al., 1999; Lohne et al., 2007; Balascio et al., 2011; Romundset et al.,2010, 2011, 2015, 2018; Vasskog et al., 2019). These studies document changes in marine influence in coastal basins during transgression and regression phases using a variety of techniques, including algal microfossil assemblages, plant and animal macrofossils, and sedimentary geochemical signatures. Elevations of isolation basin sills can be precisely surveyed using global positioning systems or LiDAR mapping.

Here we contribute to the understanding of the RSL history of the Lofoten and Vesterålen archipelagos of northern Norway (Fig. 1a). The islands are located near the continental shelf edge and the former margin of the FIS. Regional shorelines generally slope northwest reflecting an increase in former ice thickness toward the southeast. Existing RSL data recently compiled and analyzed using an ensemble of Bayesian statistical models by Creel et al. (2022) show that much of the region experienced rapid RSL fall during the late Pleistocene driven by land uplift following disintegration of the FIS. Creel et al. (2022) proposed that an episode of mid-Holocene sea-level rise (locally named the Tapes transgression) represents an interval when GMSL rise temporarily outpaced local isostatic uplift rates (see also Svendsen and Mangerud, 1987; Lambeck et al., 1998; Fjeldskaar and Bondevik, 2020). The Tapes transgression was followed by late Holocene RSL fall due to continued uplift to the present day. These trends are inferred primarily from marine and terrestrial limiting points from raised beaches, marine terraces, buried peat deposits and archaeological sites (Marthinussen 1962; Møller 1984, 1985, 1986, 1989; Vorren & Moe 1986; Vorren et al., 1988). RSL reconstructions in Norway from the early Holocene have been complicated by the presence of tsunami deposits associated with the Storegga slide, a submarine landslide along the Norwegian margin that occurred c. 8.1–8.2k cal a BP (Bondevik et al., 1997a, b, 2012). Deposits from the Storegga tsunami have not previously been reported in Lofoten or Vesterålen. However, deposits are present in some of the basins presented in this study, which is not unexpected since overwash deposits attributed to this event have been found farther north in Finnmark (Romundset and Bondevik, 2011).

The human history of Lofoten–Vesterålen has also been closely connected to past sea-level variations. For example, evidence for habitation in coastal caves on Flakstadøya in Lofoten during the mid-Holocene provides terrestrial-limiting points following the Tapes transgression, which also probably drowned many earlier archaeological sites (Møller, 1987). In the late Holocene, when more permanent agricultural communities were established, RSL changes also affected settlement locations and the accessibility of natural harbors (Balascio and Wickler, 2018). Today, the impacts of GMSL rise due to anthropogenic global warming are mitigated by continued isostatic uplift. However, in areas such as the

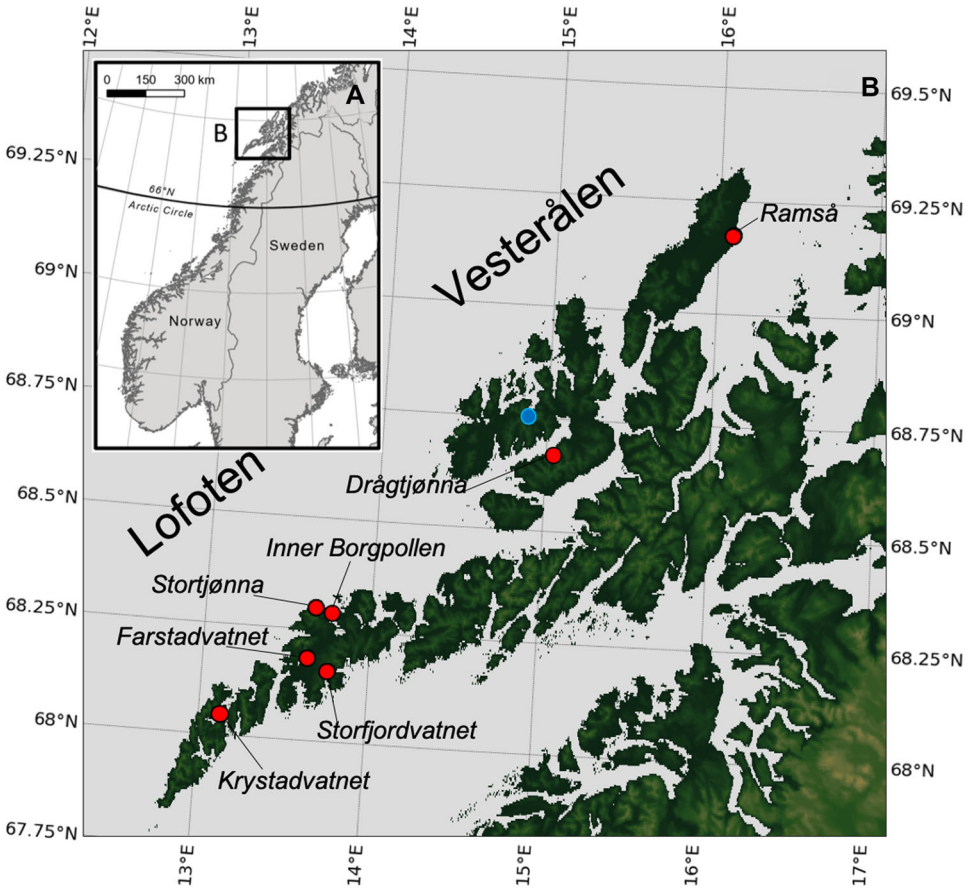


**Figure 1.** (A) The Lofoten and Vesterålen archipelagos in northern Norway. (B) Red points show the locations of isolation basins and the coastal sediment sequence near Ramså investigated as part of this study. The blue point is the average location of all Lofoten–Vesterålen RSL observations, including previously published sites, and the plotting location for the STEHME-modeled RSL curve (Table S1; Fig. 11).

Lofoten–Vesterålen archipelago, which are distal to the former FIS, uplift is already being outpaced by GMSL rise (Simpson et al., 2014).

Existing RSL data for Lofoten and Vesterålen have several limitations, including that (i) they are primarily marine or terrestrial limiting points, which less precisely constrain RSL in space and time; (ii) there are few data during the late Holocene, when human presence in the region expanded; and (iii) spatial variations between inner and outer coastal areas are poorly defined. Here we address these limitations by presenting new RSL data and spatial analyses to refine the history of Holocene RSL in Lofoten and Vesterålen. We develop seven new isolation basin SLIPs spanning the Holocene and four new limiting points derived from coastal sedimentary sequences. We identify ingression and isolation of lake basins using trends in sedimentary geochemical signatures that reflect salinity changes and water column stratification associated with different degrees of marine influence during ingression or isolation. These new index points are paired with previously published data to update the local RSL curve using an ensemble of spatiotemporal empirical hierarchical models (STEHME). This approach allows us to better constrain spatial and temporal patterns of change and assess the potential impact on our understanding of the early regional human history.

## Study sites

We investigated five isolation basins and one coastal sedimentary sequence in the study area (Fig. 1b). The isolation basins Krystadvatnet, Storfjordvatnet, Farstadvatnet and Stortjønna are located on Moskenesøya and Vestvågøya in Lofoten, and Dragtjønna is located on Langøya in Vesterålen (Fig. 2). The sill elevations of these sites range from 2.7 to 6.4 m above mean sea level (MSL). We collected additional terrestrial limiting RSL data from a transgressive stratigraphic sequence at Ramså on northern Andøya previously described by Møller (1986). This site consists of buried peat units beneath beach deposits exposed along the Gårdselva stream on the northeast coast of Andøya (Fig. 1b). We also analyzed a sediment core from Inner Borgpollen on Vestvågøya (Fig. 2). This basin has a sill elevation of 0.7 m above MSL, which is below the modern spring tidal range and therefore not fully isolated from marine influence. However, this site is significant to the early human history of the region. Inner Borgpollen was a harbor during the Iron Age (c. 2.5–0.9k cal a BP), associated with the prominent Viking Age settlement at Borg, and is surrounded by the highest concentration of Iron Age boat-houses in northern Norway. It has been hypothesized that sea-level lowering during the Iron Age affected the usefulness of Inner Borgpollen as a natural harbor (Mills et al., 2009; Balascio and Wickler, 2018). We further investigate this hypothesis through a high-resolution analysis of geochemical markers for changes in salinity and our statistical analysis of late Holocene changes in sea level throughout the region.

Our investigated sites are located on both the outer coast along the Norwegian Sea and the inner coast along Vestfjord (Fig. 1). Modern tidal amplitudes vary significantly across the region. We assess the uncertainties in tidal ranges on our reconstructions using data extrapolated from the nearest secondary ports at Andenes and Kabelvåg where the tidal

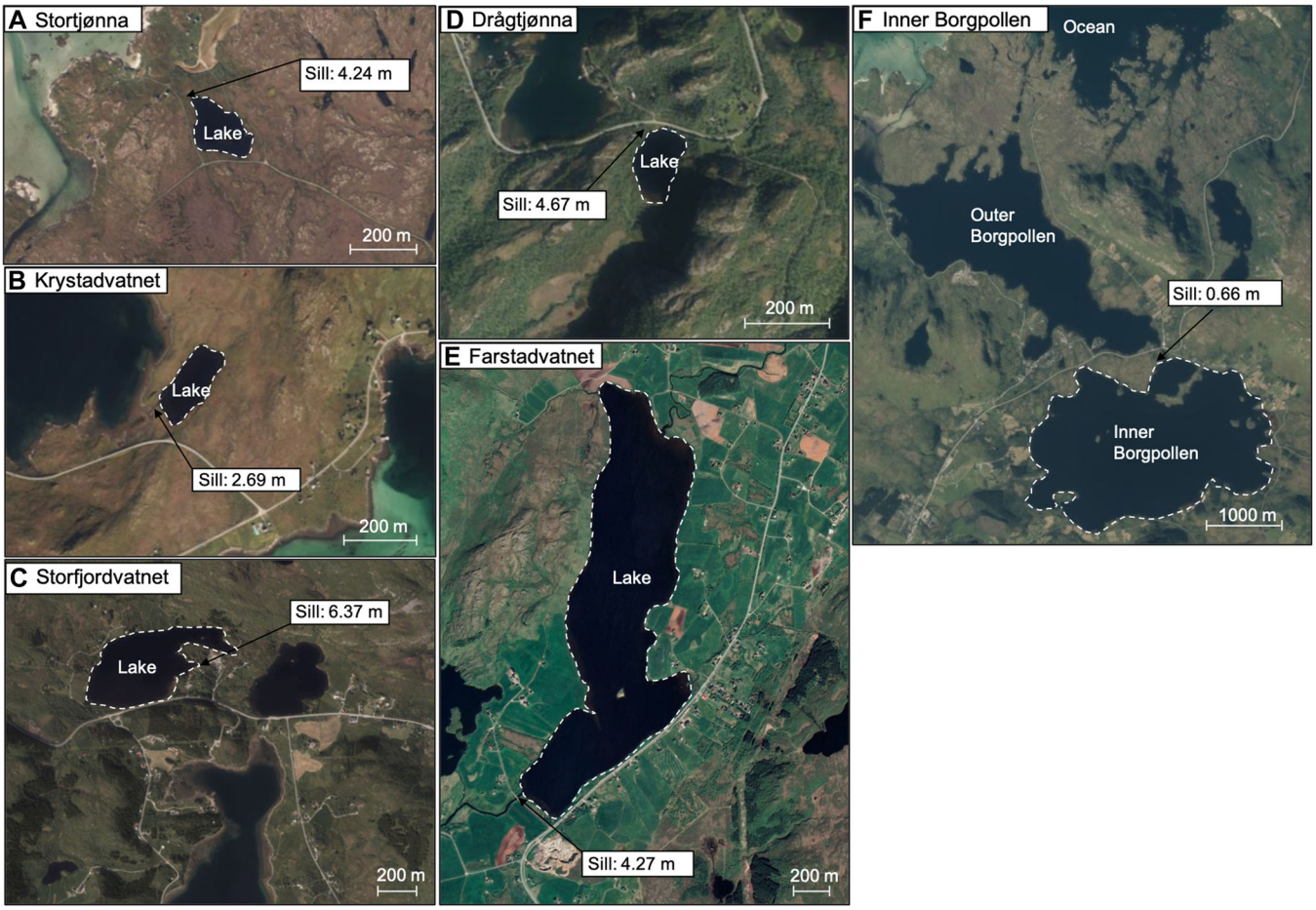


**Figure 2.** Isolation basins from Lofoten and Vesterålen (A–E) used to generate new sea-level index points and the Viking Age harbor of Inner Borgpollen (F). Sill elevations are given for each site in meters above mean sea level.

range from mean high water spring tide (MHWST) to mean low water spring tide (MLWST) is 1.78 and 2.52 m, respectively (Kartverket, 2021).

## Methods

### Field work

Field work focused primarily on the recovery of sediment cores from the deepest locations of six isolation basins. All of the basins studied have visible bedrock sills or bedrock sills mantled by boulders. Sediment cores were collected in plastic tubes using a Uwitec gravity corer or a percussion coring device, which were then packaged in the field and transported to the William & Mary Geology Department for analysis. We also collected elevation data and radiocarbon samples from the transgressive stratigraphic sequences at Ramså on northern Andøya previously described by Møller (1986).

Elevations of bedrock sills and transitions in sedimentary sequences were acquired using a Trimble GPS Pathfinder ProXRT GNSS receiver with real-time differential GPS corrections provided through OmniSTAR (DGPS). Total vertical uncertainties range from 0.507 to 0.777 m (Table 1). These uncertainties are based on the root mean squared error (RMSE) of the (i) DGPS precision, error associated with transforming height above ellipsoid measurements to the Norwegian NN2000 vertical datum; (ii) extrapolation error in estimating tidal elevations from the nearest secondary port based on the difference in MHWST and MSL between the reference port and predicted range for each site (Kartverket, 2021); and (iii) an estimated error based on the indicative meaning of isolation contacts as half the difference between mean high water neap tide (MHWNT) and the high tide level with a 1-year recurrence interval. We were unable to acquire a DGPS satellite connection at Krystadvatnet and Drågtjønna and therefore sill elevations were found using available LiDAR data and we conservatively applied a 0.50-m uncertainty range on those measurements. (Table 1).

### Sedimentary analyses for determining isolation and ingression contacts

Sediment cores were split, described and subsampled in the laboratory for a variety of sedimentary analyses. Preliminary interpretations of depositional changes and isolation contacts were based on sediment core lithology. The lithology of each core was recorded based on visual descriptions and analysis of core X-rays. Magnetic susceptibility (MS) was also measured every 1 cm along sediment cores using a Bartington MS2E sensor to determine changes in minerogenic composition. The sequence of sedimentary changes indicating changes from shallow marine to lacustrine environments were indicated by textural, color and organic matter changes. Isolation contacts were often clearly visible with finely laminated intervals, evident in X-rays. Laminated sediments indicate periods of anoxic water column conditions due to salinity stratification during and immediately following the restriction of marine input.

Total carbon (%TC), nitrogen (%N) and sulfur (%S) content was measured to identify organic matter compositional changes and track marine-derived sulfur. At all of the sites, the carbon content is primarily in organic forms, with some inorganic components represented by infrequent shell fragments during marine phases. %TC is therefore generally used to infer changes in surface water productivity, but can also indicate changes in organic matter preservation particularly during anoxic phases. %TC may also reflect input of terrestrial-derived organic matter and we use the ratio of organic carbon to nitrogen (C/N) to interpret the relative proportion of aquatic- versus terrestrial-derived organic matter. C/N values from 4 to 10 are attributed largely to algal sources and values greater than 10 are inferred to represent greater contribution from terrestrial plants (Meyers, 2003). Organic matter in these basins is typically algal-derived regardless of the phase of isolation, but higher C/N values can occur during lacustrine phases when catchment inputs have a relatively greater influence, particular in smaller basins or those in steeper catchments. Sedimentary sulfur occurs in organic and inorganic forms and is related to sulfate or sulfide concentrations in the water column and the degree of sulfate reduction, which in the presence of reduced iron can form iron sulfides (Cornwell and Morse, 1987; Mitchell et al., 1988; Holmer and Storkholm, 2001). Sulfate is a major ion in seawater, but is typically only found in trace amounts in freshwater and can be used to track marine influence in coastal environments as well as water column stratification and anoxic bottom water conditions (e.g. Jessen et al., 2008; Leng et al., 2012; Ding et al., 2016). Samples were freeze-dried and ground, and aliquots of 4–6 mg were analyzed using an Elementar vario MICRO cube element analyzer. The instrument was calibrated with sulfanilamide and the reproducibility of measurements was determined based on triplicate analysis. Average standard deviations of triplicate measurements for % TC, %N and %S were 0.3%, 0.06% and 0.04%, respectively.

Organic carbon isotope analysis ($\delta^{13}C$) was conducted as a proxy for relative changes in surface water salinity. This method is based on observations that: (i) the isotopic composition of phytoplankton can be dependent on the dominant inorganic carbon species available in surface waters (dissolved $CO_2$ vs. $HCO_3^-$) (Fogel et al., 1992); and (ii) there are typically significant differences in marine vs. freshwater plankton $\delta^{13}C$ values (e.g. Boutton, 1991; Fogel and Cifuentes, 1993; Meyers, 1994). Carbon isotopes, in combination with C/N measurements, have been applied to isolation basin studies and can be used to distinguish phases of isolation, specifically, with marine intervals having higher $\delta^{13}C$ values compared with brackish and lacustrine intervals (Westman and Hedenström, 2002; Lamb et al., 2006; Mackie et al., 2005, 2007; Mills et al., 2009; Balascio et al., 2011). Previous studies on Holocene isolation basin sequences in Scotland have defined approximate $\delta^{13}C$ ranges for marine (−16 to −22‰), brackish (−22 to −25‰) and freshwater (−25 to −30‰) conditions that correlate with microfossil-based paleo-salinities (Mackie et al., 2005, 2007). A similar relationship was found between $\delta^{13}C$ and microfossil data in a Holocene isolation basin record from Lofoten (Balascio et al., 2011). We measured carbon isotopes across the isolation sequences in each basin. To prepare samples for analysis, freeze-dried subsamples were ground and aliquots of 4–6 mg were fumigated with 10% HCl in a desiccator to remove any inorganic carbon. Samples were sent to the UC Davis Stable Isotope Facility for analysis. Results are presented using delta notation relative to a VPDB standard ($\delta^{13}C$). The uncertainty in measurements is ±0.05‰ based on the average standard deviations of triplicate analyses.

Sedimentary geochemical changes were documented at high resolution using an Itrax™ X-ray fluorescence (XRF) core scanner using a molybdenum tube and exposure time of 10 s at Lamont-Doherty Earth Observatory and the University of Bergen's EarthLab (Croudace et al., 2006; Rothwell et al., 2006). Our analysis focused on select elements to interpret changes in sediment composition and marine influence similar to how others have applied scanning XRF data in isolation basin studies (Sparrenbom et al., 2006; Balascio et al., 2011; Strunk et al., 2018; Vasskog et al., 2019).

**Table 1.** Information on isolation basins and samples from the Ramså sedimentary sequence used in establishing sea-level index points (SLIPs) and terrestrial limiting (TL) data points. Median ages, elevation adjustments and vertical uncertainties are shown for each site. Age ranges for SLIPs are based on BACON age models developed for each isolation basin record and the age ranges for TL data points are based on the 2σ calibrated age ranges for each radiocarbon sample.

| Site information | | | | | | Age control | | Elevation adjustments (m) | | | | Vertical uncertainty (m) | | | | | |
|---|---|---|---|---|---|---|---|---|---|---|---|---|---|---|---|---|---|
| Data point | Site | Latitude (°N) | Longitude (°E) | Contact | Core depth (cm) | Age (cal a BP) | Age range (cal a BP) | Height above ellipsoid | Sill/site elevation (NN2000) | Sill/site elevation (above MSL) | Sill/site elevation (above MHWST) | DGPS uncertainty | WGS84 to NN2000 | LiDAR error | Tidal interpolation | Indicative range | Total vertical uncertainty |
| SLIP-1 | Farstadvatnet | 68.184809 | 13.627431 | Ingression | 288 | 8160 | 570 | 42.74 | 4.39 | 4.27 | 3.05 | 0.152 | 0.03 | – | 0.03 | 0.71 | 0.727 |
| SLIP-2 | Stortjønna | 68.288783 | 13.760690 | Ingression | 36.5 | 7790 | 120 | 42.37 | 4.36 | 4.24 | 3.34 | 0.119 | 0.03 | – | 0.01 | 0.53 | 0.539 |
| SLIP-3 | Storfjordvatnet | 68.158814 | 13.750417 | Ingression | 240 | 7400 | 225 | 44.15 | 6.49 | 6.37 | 5.14 | 0.159 | 0.03 | – | 0.02 | 0.72 | 0.738 |
| SLIP-4 | Storfjordvatnet | 68.158814 | 13.750417 | Isolation | 32 | 5010 | 310 | 44.15 | 6.49 | 6.37 | 5.14 | 0.159 | 0.03 | – | 0.02 | 0.72 | 0.738 |
| SLIP-5 | Farstadvatnet | 68.184809 | 13.627431 | Isolation | 41 | 3850 | 250 | 42.74 | 4.39 | 4.27 | 3.05 | 0.152 | 0.03 | – | 0.03 | 0.71 | 0.727 |
| SLIP-6 | Drågtjønna | 68.669836 | 15.042177 | Isolation | 20.5 | 2500 | 190 | – | 4.80 | 4.67 | 3.78 | – | – | 0.5 | 0.00 | 0.52 | 0.721 |
| SLIP-7 | Krystadvatnet | 68.055864 | 13.139015 | Isolation | 38 | 1500 | 80 | – | 2.80 | 2.69 | 1.79 | – | – | 0.5 | 0.01 | 0.60 | 0.777 |
| TL-1 | Ramså - S3-03-19 | 69.175481 | 16.088233 | Transgressed peat | – | 11200 | 32 | 37.10 | 1.69 | 1.53 | 0.64 | 0.235 | 0.03 | – | – | 0.5 | 0.553 |
| TL-2 | Ramså - S3-02-19 | 69.175481 | 16.088233 | Transgressed peat | – | 10050 | 140 | 37.47 | 2.06 | 1.90 | 1.01 | 0.235 | 0.03 | – | – | 0.5 | 0.553 |
| TL-3 | Ramså - S3-01-19 | 69.175481 | 16.088233 | Transgressed peat | – | 8840 | 188 | 37.77 | 2.36 | 2.20 | 1.31 | 0.235 | 0.03 | – | – | 0.5 | 0.553 |
| TL-4 | Ramså - TR-01-19 | 69.174057 | 16.082057 | Transgressed peat | – | 7460 | 93 | 41.44 | 6.03 | 5.87 | 4.98 | 0.080 | 0.03 | – | – | 0.5 | 0.507 |
| TL-5 | Ramså - TR-02-19 | 69.174057 | 16.082057 | Dune stabilization | – | 5590 | 106 | 43.31 | 7.91 | 7.75 | 6.86 | 0.090 | 0.03 | – | – | 0.5 | 0.509 |

We focused on select elements to interpret changes in sediment composition and marine influence, including: sulfur (S), bromine (Br), iron (Fe) and titanium (Ti). S is interpreted to reflect changes in the input of marine-derived sulfate, similar to %S values determined by elemental analysis. We found that S normalized to calcium (Ca) values correlated best with %S values and therefore present the S/Ca ratio. Br is also interpreted as a marine-derived element. Br is an abundant ion in seawater and can be bound to organic molecules (Leri et al., 2010). Br is not present in most terrestrial environments and has been used to distinguish marine-derived organic matter in coastal sediments (Mayer et al., 1981, 2007; Ziegler et al., 2008) and used as a proxy for sea spray in coastal terrestrial environments (Schofield et al., 2010; Turner et al., 2014; Orme et al., 2015; Stewart et al., 2017). Fe and Ti can represent changes in minerogenic sediment input. Ti is a conservative element; however, Fe is redox sensitive and is soluble under low-oxygen conditions, which can occur in salinity-stratified basins as they undergo isolation. We infer Fe/Ti data as an indicator of relative changes in water column stratification.

Microscopic phytoplankton were extracted for analysis from the STOFP-118 core from Storfjordvatnet to validate the interpretations of salinity change from the geochemical methods. Eight 1-$cm^3$ samples were extracted. The samples were treated using the standard protocol for pollen sample preparation (Fægri and Iversen, 1989), which removes unwanted minerogenic and organic matter while preserving pollen and phytoplankton taxa containing sporopollenin in their cell walls. This includes marine dinoflagellate cysts and certain taxa of microscopic freshwater green algae. Taxonomic keys from Jankovská and Komárek (2000) and Komárek and Jankovska (2001) were used to identify the green algal taxa under a Zeiss light microscope, using phase contrast and a combination of a 63× objective and 12.5× oculars. Dinoflagellate cysts were assumed to be polyhalobous (marine), whereas the green algae were divided into halobian groups based on salinity tolerance as described in the online supplementary material to Vasskog et al. (2019). Isolation contacts can be recognized as a succession from samples dominated by polyhalobous (marine) taxa to samples dominated by oligohalobous indifferent and halophobous (freshwater) taxa in the core, often with a spike in halophilous (brackish/freshwater) taxa during the transition (e.g. Kaland, 1984; Vasskog et al., 2019).

### *Radiocarbon dating of isolation contacts*

Radiocarbon dating was performed on plant macrofossils picked from the surfaces of split cores and on bulk sediment samples when macrofossils were not easily isolated (Table 2). Analyses were conducted at the University of California, Irvine, Keck Carbon Cycle AMS Laboratory (UCI) and at the National Ocean Sciences AMS Laboratory at Woods Hole Oceanographic Institution (OS). Dates were calibrated to calendar years before CE 1950 (cal a BP) using CALIB version 8.20 (Stuiver et al., 2020) with the IntCal20 calibration dataset (Reimer et al., 2020). Core tops were also assigned an age based on the year of core collection, if they were recovered with the gravity corer which preserves the sediment–water interface. Age–depth models were created for each core using the Bacon age modeling software in R (Blauuw and Christen, 2011). This approach was taken to avoid interpreting the isolation ages using only select samples near the sedimentary transition, to better account for sedimentation rate changes before and after isolations, and to quantify the age uncertainty of isolation contacts.

### *Statistical modeling*

RSL was modeled using a spatiotemporal empirical hierarchical model ensemble (STEHME) following the methods of Creel et al. (2022). The seven index points and four limiting points produced here were combined with a quality-controlled, standardized database of sea level observations ($n = 1010$). An ensemble of Bayesian statistical models was trained on the sea level index points, then weighted according to each model's fit to both index and limiting points. This procedure produced a spatiotemporally continuous estimate of Norwegian RSL for the last 16 000 years. A timeseries of RSL observations in the Lofoten–Vesterålen region was then produced following the modified isobase approach of Creel et al. (2022). The average location of all Lofoten–Vesterålen RSL observations was chosen as a plotting site (68°43.765′N, 14°50.931′E; Fig. 1). For each observation, a correction term was calculated that captures the difference in RSL between the plotting site and the observation site. Adding this correction term to each RSL elevation allows plotting data from multiple locations on one time series. The correction term was calculated as the difference between the mean STEHME-modeled RSL at that observation's location and age and the mean STEHME-modeled RSL for the same age at the plotting site.

## Results

### *Farstadvatnet*

Farstadvatnet (68°11.866′N, 13°39.131′E; 1.23 $km^2$) is located on Vestvågøy, 5 km north of Leknes (Fig. 2). The lake's 17.2-$km^2$ catchment primarily drains the western side of the main agricultural valley of the island. The lake is shallow at the southwestern end, but reaches a maximum water depth of 14.5 m near its primary inlet. The sill is 4.28 m above MSL and is composed of boulders overlying bedrock, which is visible downstream from the outlet. A 337-cm composite sediment record was created by aligning geochemical data and visual stratigraphy from a 92.5-cm surface core (FSD-01-17) with two longer piston cores (FSP-01-17, 228 cm; FSP-01-18, 378 cm). We identify five stratigraphic units associated with marine and lacustrine phases of sedimentation (Fig. 3). The base of the record (Unit I; 337–291 cm) consists of a gray clayey silt that has high magnetic susceptibility and low organic content (average = 2.0%). There is a gradual transition at ~309 cm to dark brown to black sediment with millimeter-scale organic-rich laminations that continues to 291 cm. We interpret these intervals to represent lacustrine sedimentation based on low sulfur (<2%) and Br values and an average $\delta^{13}C$ of −26.5‰, excluding an anomalously high value at the very base of the record. The change in sediment texture and organic content within this unit probably indicates an increase in lake productivity during the early Holocene following regional cooling associated with the Younger Dryas.

Unit II (291–275 cm) is marked by an increase in sulfur, Fe/Ti and $\delta^{13}C$ values. At 285 cm, there is fine layer of black gyttja that generally corresponds with a broad peak in Fe/Ti and sulfur (18.5%) that is followed by an interval of rapidly rising Br and $\delta^{13}C$ values (from −27.7 to −24.3‰). This transition marks the ingression boundary and first influence of marine water into the basin associated with a brief period of water column stratification and subsequent rise in surface water salinity. The age model indicates this transition at 291 cm occurred c. $8.2 \pm 0.6$k cal a BP (Table 2). This interval corresponds with the timing of the Storegga tsunami, but no evidence for a disturbance is observed in the sediments. From 275 to 90 cm (Unit III), the sediment is generally fine-grained

**Table 2.** Isolation basin radiocarbon information.

| Site | Laboratory ID* | Composite depth (cm) | Sample name | Material dated | Radiocarbon age ($^{14}$C a BP) | Calibrated age range (cal a BP, 2σ) | Median age (cal a BP) |
|---|---|---|---|---|---|---|---|
| Krystadvatnet | | | | | | | |
| | UCI-239589 | 14.5–15 | KRD-01-17 | Terrestrial plant remains | 1435 ± 15 | 1302–1349 | 1330 |
| | UCI-226413 | 38–38.5 | KRD-01-17 | Bulk sediment | 1555 ± 15 | 1381–1515 | 1440 |
| | UCI-226412 | 39–39.5 | KRD-01-17 | Bulk sediment | 1570 ± 20 | 1395–1519 | 1460 |
| | UCI-239590 | 65–65.5 | KRD-01-17 | Terrestrial plant remains | 1935 ± 15 | 1822–1925 | 1860 |
| Farstadvatnet | | | | | | | |
| | UCI-206808 | 21–22 | FSD-01-17 | Terrestrial plant remains | 2170 ± 15 | 2113–2301 | 2243 |
| | UCI-210698 | 43–44 | FSD-01-17 | Terrestrial plant remains | 3700 ± 40 | 3908–4151 | 4038 |
| | UCI-239604 | 87.5–88 | FSD-01-17 | Bulk sediment | 4760 ± 15 | 5470–5580 | 5535 |
| | UCI-204836 | 157–158 | FSP-01-17 1/2 | Terrestrial plant remains | 5870 ± 70 | 6494–6877 | 6679 |
| | UCI-191995 | 204–205 | FSP-01-17 1/2 | Terrestrial plant remains | 5855 ± 20 | 6629–6741 | 6679 |
| | UCI-239591 | 270.5–271 | FSP-01-17 2/2 | Terrestrial plant remains | 6245 ± 25 | 7022–7254 | 7204 |
| | UCI-214458 | 286–288 | FSP-01-18 3/3 | Terrestrial plant remains | 6560 ± 220 | 6955–7911 | 7438 |
| | UCI-204837 | 311–312 | FSP-01-18 3/3 | Terrestrial plant remains | 8725 ± 25 | 9550–9885 | 9662 |
| Storfjordvatnet | | | | | | | |
| | UCI-226414 | 13–14 | SFP-01-18 1/2 | Bulk sediment | 3525 ± 20 | 3720–3880 | 3780 |
| | UCI-226415 | 26–27 | SFP-01-18 1/2 | Bulk sediment | 4110 ± 20 | 4530–4810 | 4620 |
| | UCI-220765 | 39–40 | SFP-01-18 1/2 | Bulk sediment | 4825 ± 20 | 5480–5600 | 5520 |
| | UCI-239601 | 49.5–50 | SFP-01-18 1/2 | Bulk sediment | 5150 ± 15 | 5900–5980 | 5920 |
| | UCI-239602 | 69.5–70 | SFP-01-18 1/2 | Bulk sediment | 5790 ± 15 | 6500–6660 | 6600 |
| | UCI-239603 | 99.5–100 | SFP-01-18 1/2 | Bulk sediment | 6715 ± 15 | 7520–7610 | 7580 |
| | UCI-206807 | 128–129 | SFP-01-18 1/2 | Terrestrial plant remains | 7800 ± 80 | 8410–8980 | 8590 |
| | POZ-110093 | 55–60 | STOFP-118 | Terrestrial plant remains | 4060 ± 35 | 4420–4800 | 4540 |
| | POZ-110136 | 86–89 | STOFP-118 | Terrestrial plant remains | 4835 ± 35 | 5480–5650 | 5540 |
| | POZ-110374 | 111–112 | STOFP-118 | Terrestrial plant remains | 5135 ± 35 | 5750–5990 | 5900 |
| | POZ-110137 | 233–234 | STOFP-118 | Terrestrial plant remains | 6690 ± 40 | 7480–7660 | 7560 |
| | POZ-110139 | 244–245 | STOFP-118 | Terrestrial plant remains | 7020 ± 35 | 7750–7940 | 7860 |
| | POZ-110140 | 313–316 | STOFP-118 | Terrestrial plant remains | 7960 ± 50 | 8640–8990 | 8830 |
| | POZ-110141 | 333–334 | STOFP-118 | Terrestrial plant remains | 8770 ± 50 | 9550–10120 | 9770 |
| Inner Borgpollen | | | | | | | |
| | UCI-239585 | 34–34.5 | IND-01-17 1/2 | Terrestrial plant remains | 430 ± 25 | 343–524 | 500 |
| | UCI-191997 | 56–58 | IND-01-17 1/2 | Terrestrial plant remains | 1340 ± 15 | 1179–1298 | 1290 |
| | UCI-204833 | 78–79 | IND-01-17 1/2 | Terrestrial plant remains | 1840 ± 20 | 1707–1821 | 1740 |
| | UCI-191998 | 96–97 | IND-01-17 1/2 | Terrestrial plant remains | 2335 ± 15 | 2338–2355 | 2350 |
| | UCI-204834 | 133–134 | IND-01-17 2/2 | Terrestrial plant remains | 2860 ± 110 | 2758–3324 | 3000 |
| | UCI-191999 | 172–173 | IND-01-17 2/2 | Terrestrial plant remains | 3200 ± 15 | 3383–3451 | 3420 |
| Stortjønna | | | | | | | |
| | UCI-239586 | 7–8 | SJP-01-17 | Terrestrial plant remains | 1865 ± 15 | 1725–1823 | 1770 |
| | UCI-214456 | 15–15.5 | SJP-01-17 | Terrestrial plant remains | 1635 ± 20 | 1413–1547 | 1520 |
| | UCI-239587 | 25–26 | SJP-01-17 | Terrestrial plant remains | 6205 ± 15 | 7007–7166 | 7080 |
| | OS-139111 | 36.5–37 | SJP-01-17 | Terrestrial plant remains | 6860 ± 75 | 7574–7913 | 7700 |
| | OS-139111 | 36.5–37 | SJP-01-17 | Terrestrial plant remains | 7080 ± 95 | 7681–8160 | 7890 |

(*Continued*)

**Table 2.** (*Continued*)

| Site | Laboratory ID* | Composite depth (cm) | Sample name | Material dated | Radiocarbon age ($^{14}$C a BP) | Calibrated age range (cal a BP, 2σ) | Median age (cal a BP) |
|---|---|---|---|---|---|---|---|
| Drågtjønna | | | | | | | |
| | UCI-239600 | 10–10.5 | DRP-01-19 | Bulk sediment | 2145 ± 15 | 2053–2294 | 2130 |
| | UCI-226392 | 21–22 | DRP-01-19 | Terrestrial plant remains | 2410 ± 25 | 2351–2673 | 2430 |
| | UCI-226391 | 27–27.5 | DRP-01-19 | Terrestrial plant remains | 2765 ± 20 | 2782–2929 | 2850 |
| | UCI-239588 | 38.5–39 | DRP-01-19 | Terrestrial plant remains | 2505 ± 20 | 2494–2723 | 2580 |

*UCI – University of California Irvine Keck-CCAMS Facility, USA; OS – National Ocean Sciences AMS Facility, USA; POZ – Poznan Radiocarbon Laboratory, Poland.

and dark brown, and with dispersed shell fragments throughout representing marine conditions. Across this unit, sulfur values rise from c. 4 to 10% and $\delta^{13}$C values remain elevated (average −23.4‰). At 90 cm we interpret a brackish phase (90–41 cm; Unit IV) marked by lower $\delta^{13}$C values to indicate a decrease in salinity and elevated %S and Fe/Ti values to suggest greater stratification of the water column. Above 41 cm, $\delta^{13}$C values decrease to less than c. −28‰, typical of freshwater conditions and the sediment transitions to a dark brown to black gyttja with abundant plant macrofossils (41–0 cm; Unit V). This transition at 41 cm is also marked by an abrupt decrease in Fe/Ti and %S to values less than 1.0%. Our age model indicates that the isolation at 41 cm dates to 3.9 ± 0.3k cal a BP (Fig. 3; Table 1).

## *Storfjordvatnet*

Storfjordvatnet (68°9.488′N, 13°44.574′E; 0.18 km$^2$) is located on the southern side of Vestvågøy, 6 km east of Leknes (Fig. 2). The lake has a 4.3-km$^2$ catchment and a maximum water depth of 10.7 m, and is surrounded by steep slopes with elevations reaching c. 450 m. The lake's outlet flows to the east over a bedrock sill with an elevation of 6.49 m above MSL. Two piston cores were recovered from the deepest part of the lake: SFP-01-18 (140 cm) and STOFP-118 (495 cm) (Figs. 4 and 5).

In core SFP-01-18, we identify three stratigraphic units associated with marine, brackish and lacustrine phases of sedimentation (Fig. 4). Unit I (140–63 cm) consists of a dark brown silty mud with shell fragments throughout, representing marine conditions. The lower 16 cm of this Unit is a gray, clayey silt characterized by low organic content and high magnetic susceptibility values. This marine interval is characterized by elevated Br, gradually increasing %S (4–5%) and $\delta^{13}$C values that range from −25 to −20‰. At 63 cm there is a transition to Unit II (63–32 cm) where $\delta^{13}$C and Br values decline indicating a decrease in surface water salinity and this is accompanied by a sharp increase in Fe/Ti and %S, indicators of water column stratification. $\delta^{13}$C values reach values typical of freshwater conditions (less than −28‰) at 40 cm, but %S, Br and Fe/Ti values remain elevated, indicating prolonged stratification and periodic marine influence until 32 cm when the basin became fully isolated. At 32 cm there is an abrupt decrease in %S and Fe/Ti, and Br and $\delta^{13}$C values remain below −28‰ (Unit III; 32–0 cm). Seven radiocarbon dates define sedimentation rates and a Bacon age model was used to interpolate the age of the isolation at 32 cm to 5.0 ± 0.3k cal a BP (Fig. 4; Table 1).

Core STOFP-118 spans the entire Holocene and parts of the Late Glacial, and we identify five stratigraphic units associated with marine, brackish and lacustrine phases of sedimentation (Fig. 5). Unit I (495–360 cm) is a dense, gray, minerogenic silt that is faintly laminated and characterized by high magnetic susceptibility values. The upper c. 30 cm of this unit is strongly laminated, has a decreasing trend in magnetic susceptibility, and hs peaks in S/Ca and Br values, which decline sharply at the base of Unit II. We interpret the gray, minerogenic silt in Unit I to reflect glacier input to the lake in the early Holocene that decreases in the upper part of Unit I when the basin probably had some marine influence, as indicated by the interval of higher Br and S/Ca values. The transition to Unit II probably represents the onset of lacustrine conditions, but we lack the chronologic control to confidently document an age for this first isolation. Unit II (360–240 cm) represents an interval of lacustrine sedimentation, defined by low S/Ca, Br and Fe/Ti values. Select phytoplankton samples also suggest freshwater conditions. Sedimentation in Unit II is interrupted

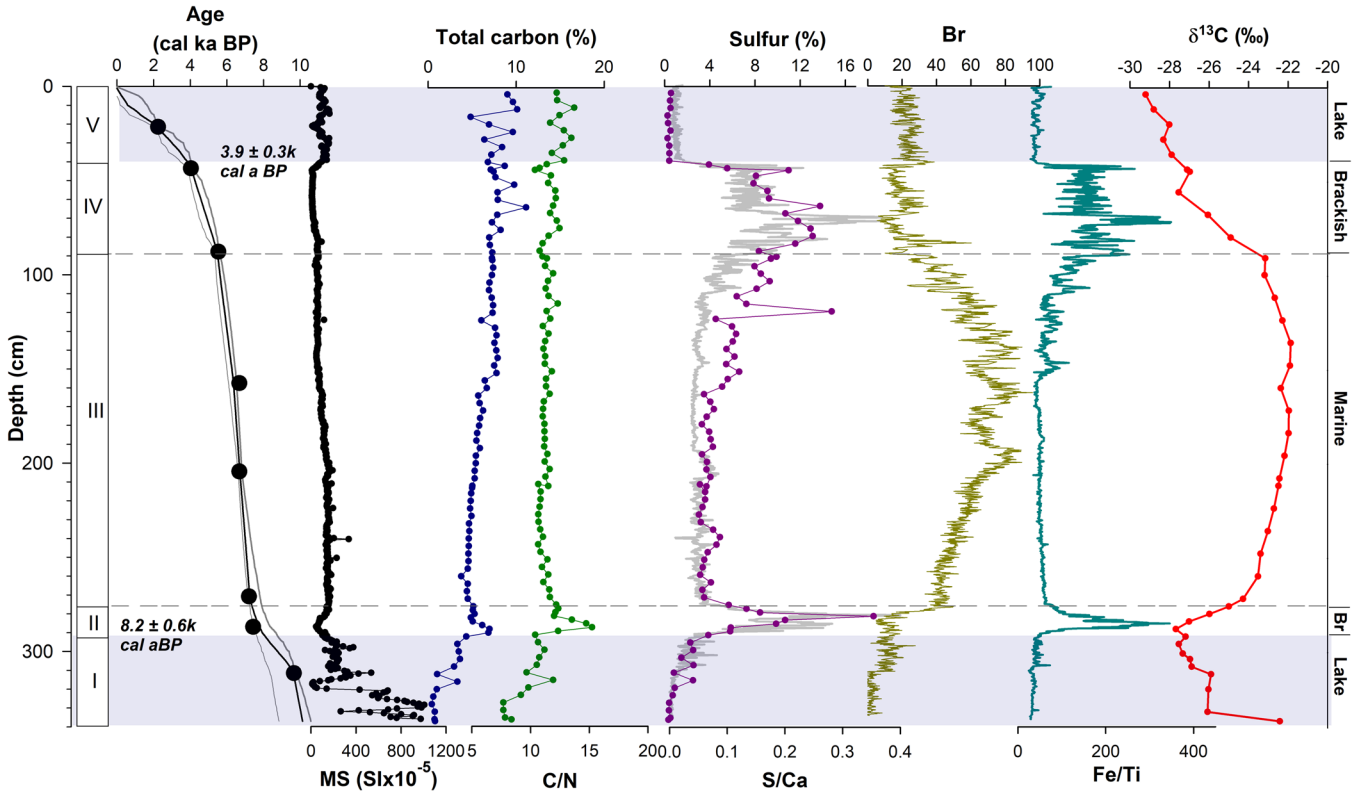


**Figure 3.** Stratigraphic, geochemical and chronologic data from the Farstadvatnet record identifying marine, brackish (Br) and lacustrine phases. An ingression contact is identified at 8.2k cal a BP and an isolation contact at 3.9k cal a BP.

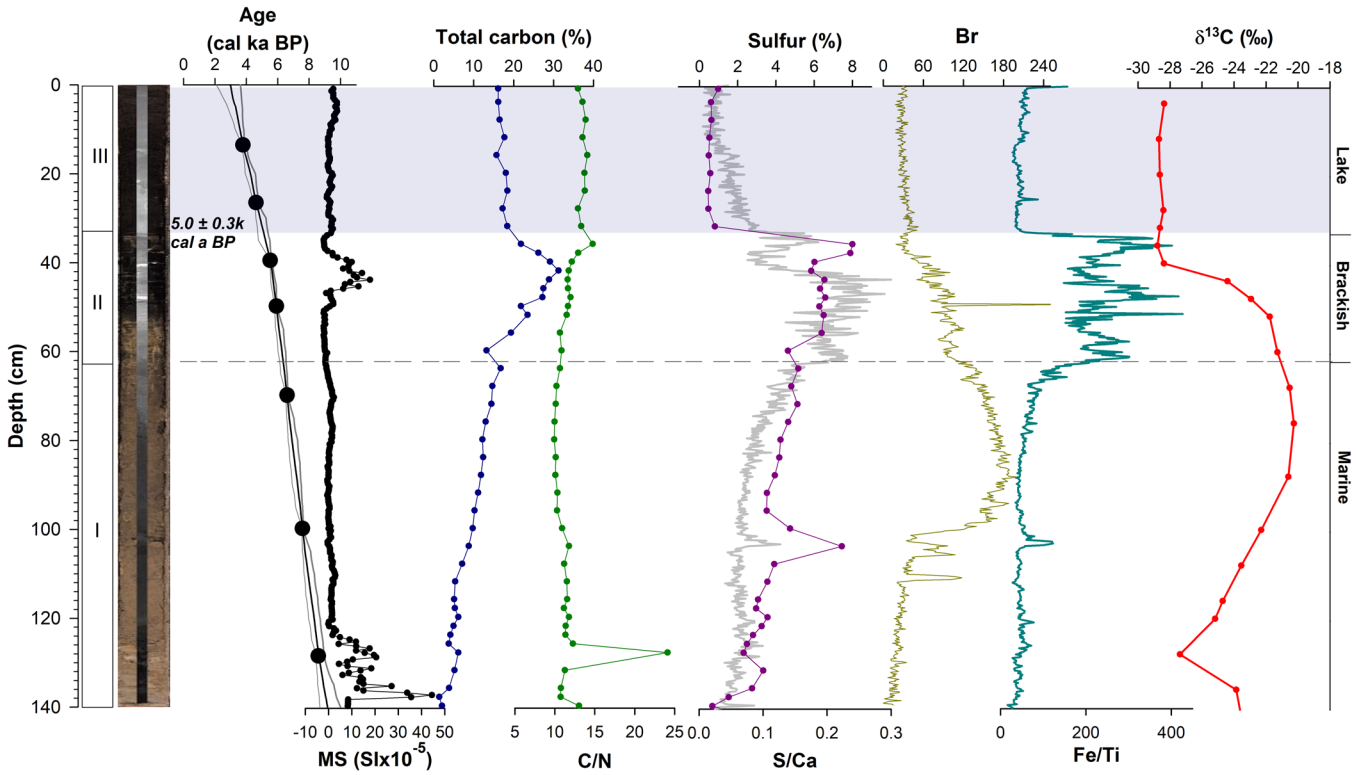


**Figure 4.** Stratigraphic, geochemical and chronologic data from the Storfjordvatnet record SFP-01-18 identifying marine, brackish and lacustrine phases. An isolation contact is identified at 5.0 cal a BP.

by an event deposit clearly visible in the core from 315 to 255 cm. This deposit has a sharp basal contact where the sediment transitions from gyttja to sand, which contains rip-up clasts of silt and gyttja and that fines upward. Based on these sediment characteristics, as well as the radiocarbon age at the top of this deposit (7.9k cal a BP), we attribute this deposit to the Storegga Tsunami (Bondevik et al., 2012). Unit III (240–118 cm) represent a transition to marine conditions. There is a sharp increase in S/Ca, Br and Fe/Ti and phytoplankton samples show higher concentrations of

salinity-tolerant species. The age model for this core indicates this lacustrine–marine transition at 240 cm occurred c. 7.4 ± 0.2k cal a BP (Fig. 5; Table 1). The most recent lithologic units III, IV and V in STOFP-118 correspond to Units I, II and III in core SFP-01-18. Both records display similar trends in S/Ca, Br and Fe/Ti values and the association of these units with marine, brackish and lacustrine phases, respectively, is confirmed by phytoplankton data. The age of the final isolation in STOFP-118 at 62 cm is dated to 4.8 ± 0.3k cal a BP, which is within the uncertainty of the isolation age independently identified in SFP-01-18. However, we use the date from SFP-01-18 as the inferred isolation age (5.0 ± 0.3k cal a BP) for Storfjordvatnet in our regional reconstruction since it is constrained with a greater number of radiocarbon ages above and below the isolation contact.

## *Drågtjønna*

Drågtjønna (68°40.143′N, 15°2.574′E; 0.02 km$^2$) is located along Eidsfjord on Langøy in Vesterålen (Fig. 2). The lake is 7.2 m deep and within a steep 0.28-km$^2$ catchment with surrounding peaks that reach ~200 m in elevation. The bedrock threshold that impounds the lake is 4.66 m above MSL. The isolation of the basin is captured in a 60-cm surface core (DRP-01-19) (Fig. 6) The sediment is mostly a dark brown to black, fine-grained sediment, but the lowest 18 cm contains coarse sand and some pebbles. We interpret the lower 30 cm to represent marine conditions defined by high $\delta^{13}$C values (mean = −21.0‰), high %S (mean = 5.1%), and elevated Br and Fe/Ti values. From 30 to 20.5 cm we interpret brackish conditions based on the onset of a decline in $\delta^{13}$C values and an increase in %S and Fe/Ti. The rapid decline in $\delta^{13}$C values stabilizes at 24 cm (−29.5‰) indicating fresh surface water conditions, but %S and Fe/Ti values remain elevated to 20.5 cm showing water column stratification and periodic marine influence. Freshwater conditions from 20.5 to 0 cm are inferred from %S values less than 1.5%, low Fe/Ti and Br values, and $\delta^{13}$C values lower than −29‰. Four radiocarbon dates, including one within 1 cm of the isolation contact, were used to define sedimentation rates. The age model indicates that the isolation at 20.5 cm occurred c. 2.5 ± 0.2k cal a BP (Fig. 6; Table 1).

## *Krystadvatnet*

Krystadvatnet (68°3.383′N, 13°8.479′E; 0.02 km$^2$) is located along the inner part of Torsfjord on Moskenesøya (Fig. 2). The lake has a 0.13-km$^2$ catchment, a maximum water depth of 3.7 m and a clear bedrock threshold that is 2.69 m above MSL. The isolation of the basin is captured in a 70-cm core (KRD-01-17) (Fig. 7). The sediment is organic-rich and fine grained throughout the core. However, the lowest 31 cm (Unit I; 70–39 cm) is characterized by distinctly higher %S (3–13%), Br and Fe/Ti values, as well as moderately higher $\delta^{13}$C values (−26.4 to −24.3‰). At 39 cm there is a sharp decline in %S to values less than 1.4% and lower average $\delta^{13}$C values (less than −26.4‰). We interpret conditions from 70 to 39 cm (Unit II) to represent a brackish phase immediately prior to isolation based on the high sulfur and Fe/Ti values, and the moderately high $\delta^{13}$C values. Four radiocarbon dates, including two within 1 cm of the isolation contact, were used to define sedimentation rates. The age model indicates that the isolation at 39 cm occurred c. 1.5 ± 0.8k cal a BP (Fig. 7; Table 1).

## *Stortjønna*

Stortjønna (68°17.324′N, 13°45.643′E; 3.46 km$^2$) is a small lake ~3 m deep located in a bedrock-controlled basin in a low-relief catchment between Outer Borgpollen and the ocean (Fig. 2). The threshold that impounds the lake is 4.25 m above MSL. A 46.5-cm percussion core (SJP-01-17) was recovered from the center of the lake and contains four lithostratigraphic units that we interpret to represent ingression and isolation of the basin (Fig. 8). In Unit I (46.5–36.5 cm), the sediment is

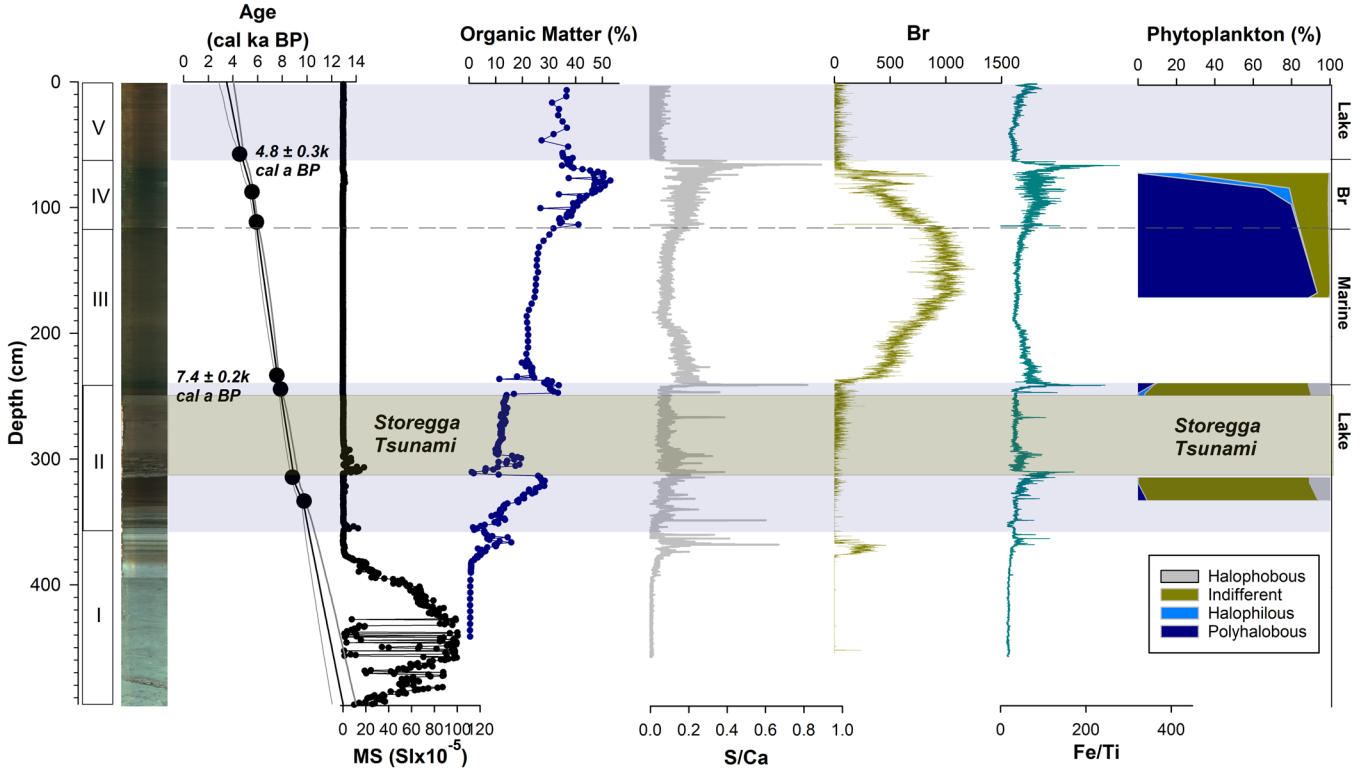


**Figure 5.** Stratigraphic, geochemical, phytoplankton and chronologic data from the Storfjordvatnet record STOFP-118 identifying marine, brackish (Br) and lacustrine phases. An ingression contact is identified at 7.4k cal a BP and an isolation contact at 4.8k cal a BP.

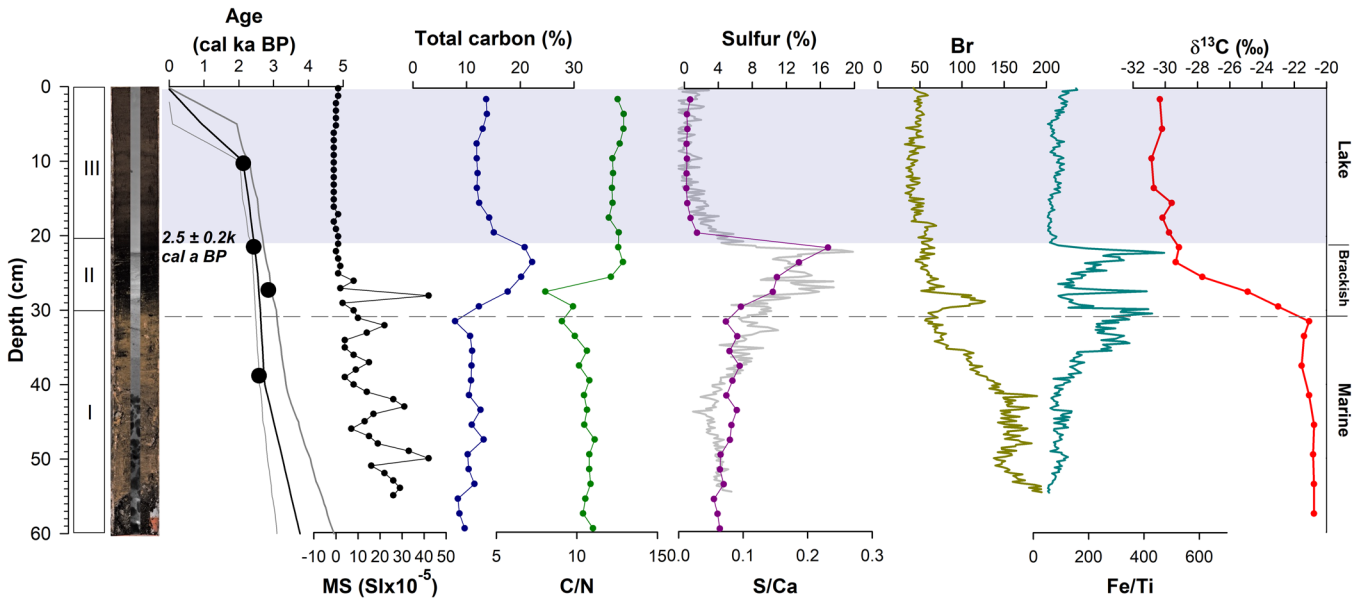


**Figure 6.** Stratigraphic, geochemical and chronologic data from the Dragtjønna record identifying marine, brackish and lacustrine phases. An isolation contact is identified at 2.5k cal a BP.

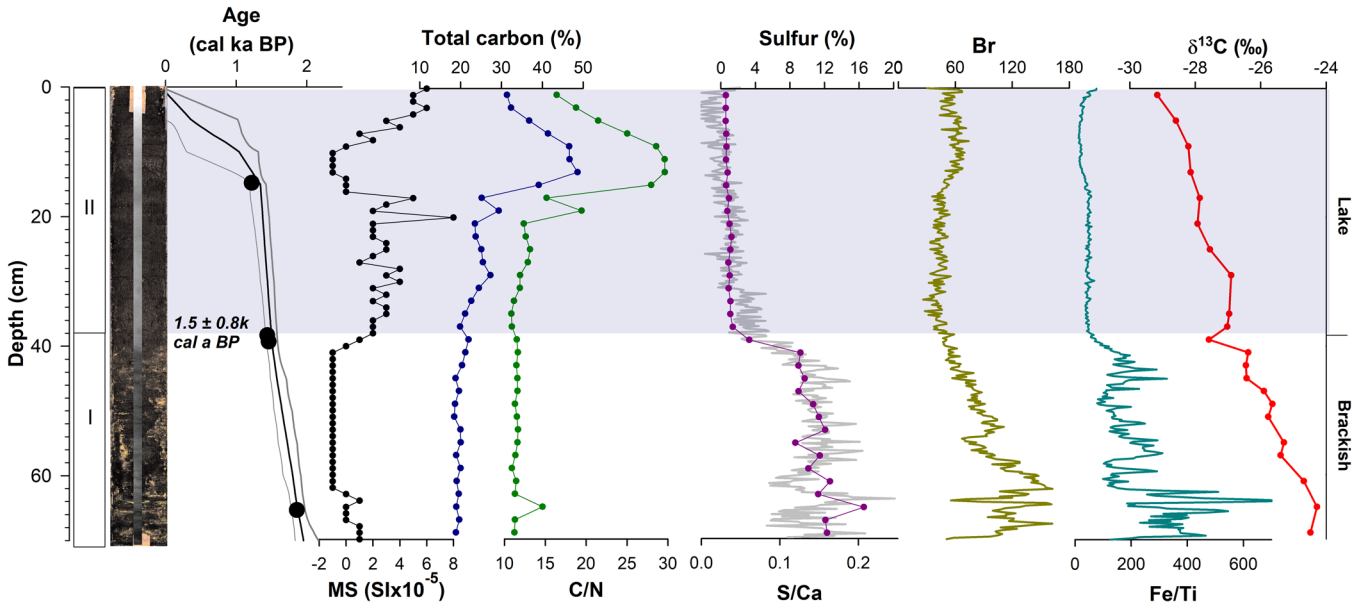


**Figure 7.** Stratigraphic, geochemical and chronologic data from Krystadvatnet identifying brackish and lacustrine phases. An isolation contact is identified at 1.5k cal a BP.

composed of coarse sand to fine gravel with numerous shell fragments. At 36.5 cm there is a sharp transition to a dark-brown, fine-grained, organic sediment. Unit I potentially represents a marine overwash deposit based on its course-grained texture, presence of broken shell material and abrupt transition to organic-rich sediment. Two radiocarbon ages at 36.5 cm (7.7 and 7.9 cal a BP; Table 2) also indicate that it was deposited around the time of the Storegga Tsunami (Bondevik et al., 1997). Unit II (36.5–31.5 cm) is marked by higher %C, %S and Fe/Ti values and relatively low Br and $\delta^{13}C$ (average −27‰) indicating brackish conditions or a period of recovery following the tsunami. Unit III (31.5–15.5 cm) represents a clear transition to marine conditions defined by lighter brown sediment, a decrease in %C, %S and Fe/Ti, and higher Br and $\delta^{13}C$ values, which reach −18‰. The chronology indicates that ingression occurred c. 7.8 ± 0.1k cal a BP (Fig. 8; Table 1). The transition to Unit IV (15.5–0 cm) represents isolation of the basins and is marked by a decrease in Br and lower $\delta^{13}C$ values. The chronology associated with isolation is highly uncertain because of an abrupt change, or possible hiatus, in sedimentation so we refrain from assigning an isolation age for this basin.

## *Inner Borgpollen*

Borgpollen consists of two deep coastal basins near present sea level (Inner and Outer Borgpollen) that extend ~7 km inland from the north coast of Vestvågøy (Fig. 2). They are both restricted coastal marine basins. A narrow and shallow channel separates Inner and Outer Borpollen, and two narrow channels connect Outer Borgpollen to the ocean. Inner Borgpollen (68°14.865′N, 13°49.107′E; 4.35 $km^2$) drains a ~ 37.2-$km^2$ catchment, is 45 m deep and is meromictic with anoxic bottom water. Water column data show that the base of

the summer thermocline and oxycline are at ~20 m, and the salinity ranges from ~3 ppt at the surface to ~7 ppt at depth. A 176-cm gravity core (IND-01-17) was recovered from the deepest part of Inner Borgpollen. We identify three stratigraphic units associated with changes in marine influence from marine to brackish conditions (Fig. 9). The base of the record (Unit I; 176–67 cm) is dense, light brown, organic sediment with faint color banding. Geochemical properties indicate marine conditions as characterized by relatively high $\delta^{13}C$ values (mean = −21.2‰), and increasing Fe/Ti and %S values, from 6 to 12%. In Unit II (67–30 cm), the sediment transitions to a less dense, dark brown, weakly laminated, organic sediment. The characteristics of this unit indicate the onset of brackish conditions marked by elevated Fe/Ti and %S values (mean = 12%), and a decreasing trend in $\delta^{13}C$ values from −21.9 to −24.7‰. The upper 30 cm is a very low density, black, organic-rich sediment marked by a continued decline in $\delta^{13}C$ values and %S, and lower Br and Fe/Ti values. We interpret the change in sediment characteristics at 67 cm to indicate the onset of brackish conditions and a significant decrease in surface water salinity and an associated increase in water column stratification, as represented by the decline $\delta^{13}C$

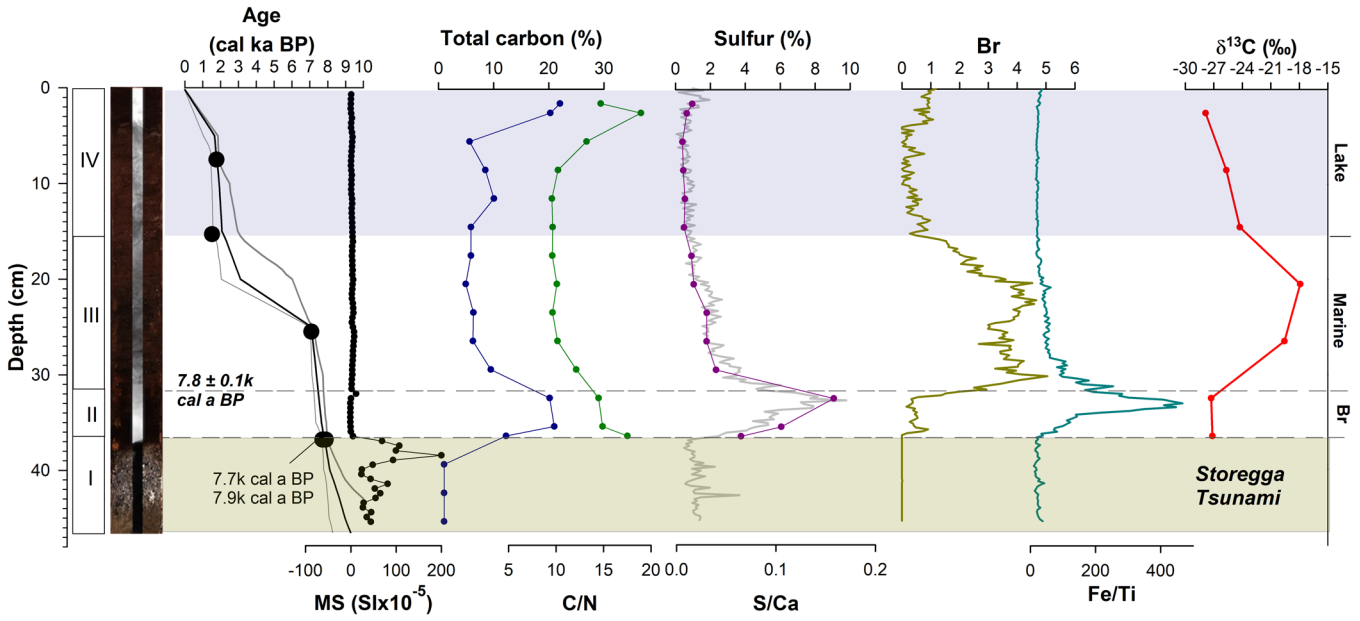


**Figure 8.** Stratigraphic, geochemical and chronologic data from the Storjønna record identifying marine, brackish (Br) and lacustrine phases. An ingression contact is identified at 7.8k cal a BP.

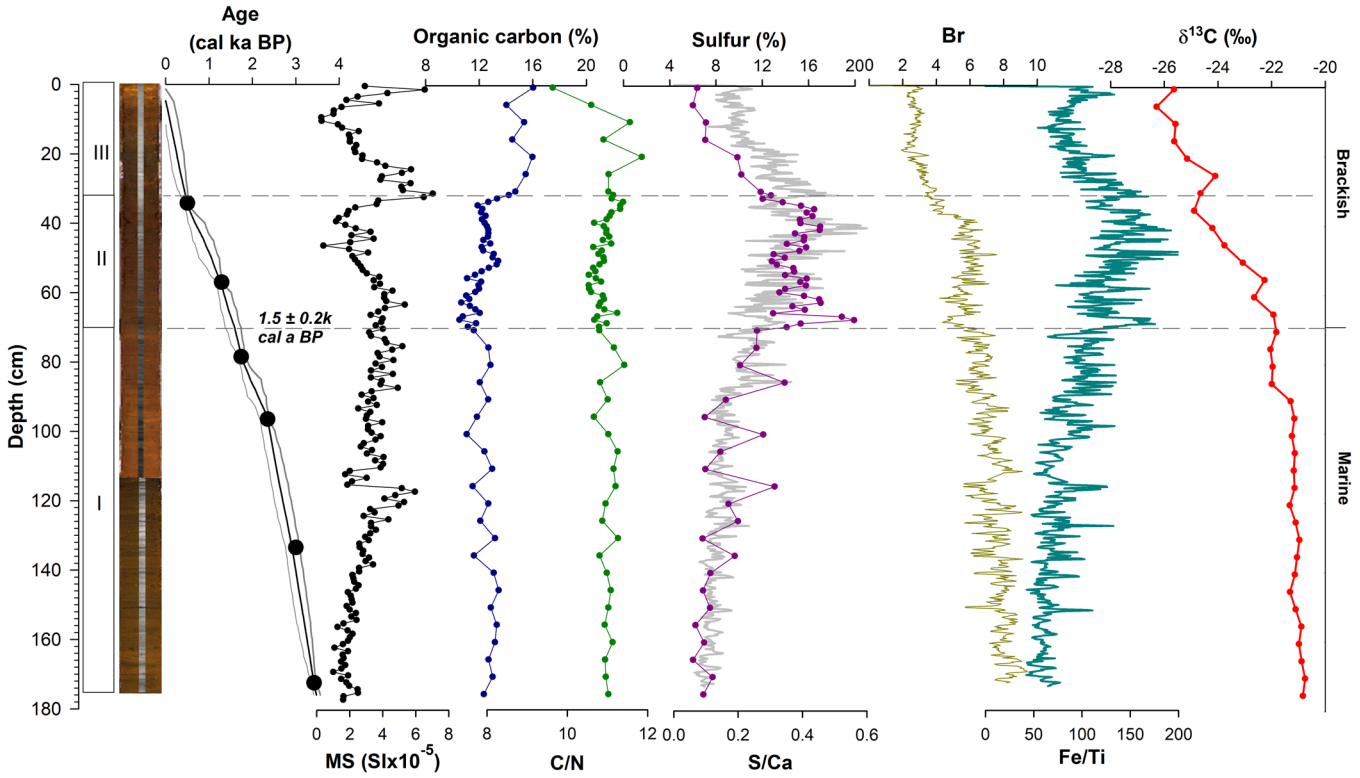


**Figure 9.** Stratigraphic, geochemical and chronologic data from the Inner Borgpollen record identifying marine and brackish phases. A transition to brackish conditions is identified at 1.5k cal a BP.

values and increase in %S. Further restriction of the basin occurred at ~30 cm when Br values sharply drop and $\delta^{13}C$ values continue to decrease, although geochemical data also indicate brackish conditions. The age model indicates that the onset of the transition in water column conditions at 67 cm dates to 1.5 ± 0.2k cal a BP (Fig. 9).

### *Ramså coastal sedimentary sequence*

A transgressive sequence exposed along the Gårdselva stream at Ramså on northern Andøya has provided important constraints on the local sea-level history (Holmboe, 1903; Marthinussen, 1962; Møller, 1986). We revisited the stratigraphic section S3 (69.175481°N, 16.088233°E) described by Møller (1986), which consists of peat overlain by a beach deposit. Similar to Møller's (1986) description, we observed the base of the sequence near the stream bed as composed of sand with thin organic lenses grading into a 60-cm-thick dense peat unit overlain by sand and rounded cobbles. The elevation of the contact between the peat and beach deposit is 2.20 m above MSL. We collected three samples from throughout the underlying peat for microscopic analysis and radiocarbon dating (Tables 1 and 3). The lowest elevation sample (S3-03-19) is from 67 cm below the contact between the peat and beach deposit near the base of the exposure. The sample is composed of very fine organic debris and fine sand mixed with some bryophytes and fruits of the shallow-water aquatic plant *Najas* (water nymph) indicating a moist and possibly lacustrine environment. A radiocarbon date of mixed fine plant parts and bryophytes yielded an age of 11.17–11.24k cal a BP. The sample from the middle of the peat deposit (S3-02-19) is highly compressed peat with almost no sand and many woody fragments (probably birch; *Betula* sp.) that have a radiocarbon age of 9.9-–10.2k cal a BP. The sample from immediately underlying the beach deposit (S3-01-19) is a highly compressed peat with many organic fragments and seeds of *Menyanthes* (buckbean), and almost no sand. A sample of wood fragments and plant stems from this sample yielded an age of 8.7–9.0k cal a BP.

We also investigated a 3-m-deep trench (69.174057°N, 16.082057°E) located 250 m west of section S3 that was excavated for drainage as part of road construction (Table 3). The base of the deposit consists of sand with thin peaty organic lenses, similar to the base of section S3, that abruptly transitions to what we interpret is a c. 2-m-thick aeolian sand unit that is capped by peat lenses. The elevation of the contact between the uppermost peat lens and aeolian sand is 5.87 m above MSL. Analysis of a sample from the uppermost peat lens (TR-01-19) shows that it contains a mixture of organic debris and fine sands, with numerous twigs, wood fragments, leaves and twigs of bryophytes, and beetle elytra, which all suggest deposition in a moist terrestrial environment (Tables 1 and 3). A sample of mixed wood fragments from this deposit has an age of 7.4–7.6 cal a BP. The elevation of the contact between aeolian sand and overlying peat is 7.75 m above MSL. A sample from this upper peat (TR-02-19) had similar characteristics to TR-01-19 and a mix of sedge (Cyperaceae) culms and small wood fragments date to 5.5–5.7k cal a BP (Tables 1 and 3).

## Discussion

### *Geochemical characteristics of isolation basin sequences*

Geochemical changes observed within our isolation basin sediment records reveal several consistent trends associated with ingression and isolation sequences. Similar to other studies, marine conditions were most evident in our records based on elevated $\delta^{13}C$ values, %S and Br values. The range of $\delta^{13}C$ values for marine (c. −20 to −23‰), brackish (c. −23 to −26‰) and freshwater (c. −23 to −26‰) that we found (Fig. 10a) are similar to the range of values reported in other studies (Mackie et al., 2005, 2007; Balascio et al., 2011). Slight variations in $\delta^{13}C$ values among the marine phases in our records can be attributed to minor salinity differences in the range of inner and outer coastal environments of our sites. In addition to observing changes in surface water salinity as interpreted from $\delta^{13}C$ values, we also show how %S and S/Ca values reflect changes in marine influence and water column stratification. Lacustrine conditions are associated with %S measurements with values less than c. 2% in all freshwater intervals, and we found that considering %S together with $\delta^{13}C$ values provides a clearer distinction between changes in surface water conditions and water column stratification (Fig. 10b). These intervals are also characterized by lower Br, Fe/Ti and $\delta^{13}C$ values. Brackish conditions were inferred as intervals with declining $\delta^{13}C$ values between lacustrine and marine units and often associated with periods of salinity stratification. We interpret water column stratification to indicate periodic marine input, which would be required to maintain these conditions, and define isolation when the water column is no longer stratified. Inner Borgpollen provides an analog, as it remains tidally influenced, has a stratified water column and has surface water salinity that has been declining since c. 1.5k cal a BP. Water column stratification is defined by distinctly higher %S, S/Ca and Fe/Ti values reflecting anoxic conditions near the bottom of the basins. The elevated %S and Fe/Ti values that characterize these intervals can be explained by conditions favorable for the precipitation of iron sulfide

**Table 3.** Biotic remains found in samples from the Ramså coastal sedimentary sequence.

| | | Biotic indicator | | | | | | | | |
|---|---|---|---|---|---|---|---|---|---|---|
| Site | Sediment type | *Rubus* | Bryophytes | *Menyanthes* | *Najas* | Beetle elytra | *Hydrozetes* | Trichoptera | Carbonaceaous spheres | Wood fragments |
| Ramså S3 | Peat | | | | | | | | | X |
| Ramså S3-01-19 | Peat | | | X | | | | | X | |
| Ramså S3-02-19 | Peat | | | | | X | | | | X (*Betula*) |
| Ramså S3-03-19 | Fine organics, fine sands | | X | | X | | | | | |
| TR-01-19 | Fine organics, fine sands | | X | | | X | X | | X | X |
| TR-02-19 | Fine organics, sand | | | | | X | | | | |

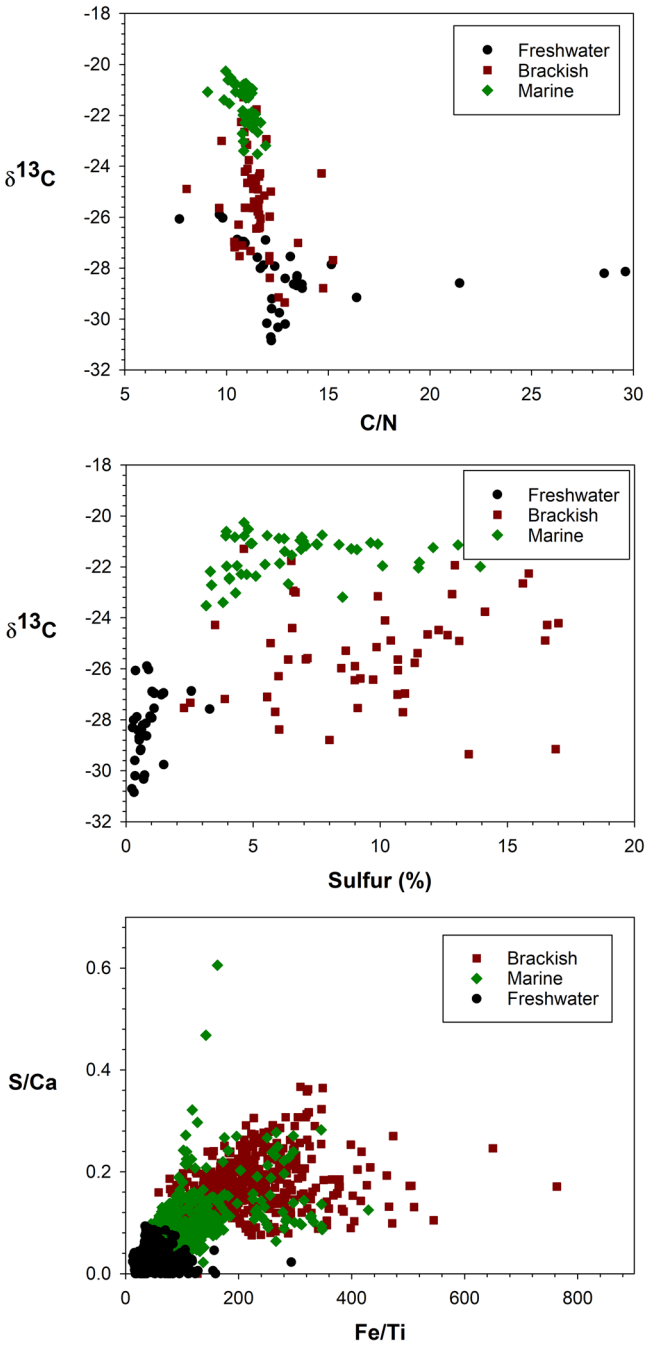


**Figure 10.** Geochemical data used to distinguish marine, brackish and lacustrine conditions in isolation basin records.

minerals (e.g. pyrite, mackinawite, greigite, amorphous-FeS) typically found in marine anoxic environments when sulfide and reduced iron are abundant (Cornwell and Morse, 1987). Comparison of XRF-derived S/Ca and Fe/Ti values show how these elemental ratios can also be used to distinguish isolation phases with much higher resolution (Fig. 10c). Our interpretations of the phases of basin isolation, made based on geochemical data, are further supported by analysis of phytoplankton data from Storfjordvatnet, which is a more traditional approach and verifies trends in reconstructed salinity changes.

## *Indicative meanings and sea-level index points*

The indicative meaning of isolation and ingression contacts in coastal basins depends on their coastal setting, geomorphic characteristics and freshwater inputs (Corner et al., 1999; Shennan et al., 2000). Isolation and ingression contacts in this study have been assigned MHWST as their indicative meaning, and we use an indicative range from MHWNT to the high tide level with a 1-year recurrence interval to account for these uncertainties. The indicative range employed here differs from, but is encompassed by, the wider range of (MHWST+MLWST)/2 applied by Creel et al. (2022). This tighter indicative range more accurately reflects basin sill positions relative to sea level at these locations. Our analysis yields seven new SLIPs based on the interpretation of ingression and isolation contacts from five isolation basins that constrain sea level from 8.2 to 1.5k cal a BP (Table 1).

The indicative meaning of sedimentary indictors depends on their stratigraphic positions relative to transgressive or regressive contacts. The buried peat samples from Ramså represent freshwater terrestrial environments that were transgressed by beach deposits and therefore yield maximum limiting ages for transgression. We assign these limiting data points an indicative meaning of greater than MHWST (Table 1). The peat sample from above the aeolian sand represents the stabilization of dunes following the Tapes transgression maximum and therefore provides a minimum limiting age and elevation for the subsequent regression. We assign this limiting data point an indicative meaning of greater than MHWST (Table 1). These results generally support data presented by Møller (1986) for the Ramså sequence and provide additional terrestrial limiting data points to use in constraining the regional sea-level history.

## *Spatio-temporal analysis of Holocene sea-level trends for Lofoten–Vesterålen*

Holocene relative sea-level data from Lofoten–Vesterålen were compiled and evaluated using an STEHME with Gaussian process regression following the approach presented in Creel et al. (2022) (Fig. 11). The benefits of this approach are that it utilizes all sources of RSL data, accounts for both temporal and vertical uncertainty, and allows for improved spatial mapping of regional sea-level trends. The new SLIPs and terrestrial limiting points produced in this study were used to generate the STEHME along with previously published data from isolation basins, peat deposits, raised beaches, a marine terrace and dated cultural horizons from archaeological sites (Marthinussen, 1962; Nydal et al., 1964; Møller, 1984, 1986; Vorren et al., 1988; Vorren, 1978; Vorren and Moe, 1986; Balascio et al., 2011; Midtun, 2019; Vetti, 2020) (Table S1; Fig. S1). An RSL timeseries for the region was generated based on a modified isobase approach that uses the STEHME to adjust RSL index points to a common location (see Creel et al., 2022) (Fig. 11).

The STEHME for Lofoten–Vesterålen shows a lowstand in the early Holocene from c. 12 to 9k cal a BP with RSL elevations below present (Fig. 11). The lowstand is primarily constrained by buried and submerged peat deposits from sites in Lofoten and Vesterålen (Marthinussen, 1962; Nydal et al., 1964, 1972; Vorren and Moe, 1986; Møller, 1984, 1986) and further supported by our new ages on the buried peat deposit from the Ramså sequence (Table 2). The mid-Holocene Tapes transgression occurs from c. 9 to 6k cal a BP when the STEHME mean increases from c. −4 to 7 m above present-day RSL with a maximum at c. 7 cal a BP. The transgression is constrained by ingression dates on Farstadvatnet, Stortjønna and Storfjordvatnet (Figs. 3, 4, 5 and 8) in addition to previously published isolation basin data (Balascio et al., 2011), transgressed peat deposits (Marthinussen, 1962; Nydal, 1962; Møller, 1984, 1986) and a date on a raised beach (Møller, 1984). Following the transgression maximum, there is a continuous RSL fall from 6 to 5k cal a BP with the STEHME mean decreasing to 4 m above present-day RSL. Over the last 5k cal a BP, RSL more gradually declined at an average rate of c. 0.8 m $ka^{-1}$. RSL fall over the last 6k cal a BP is

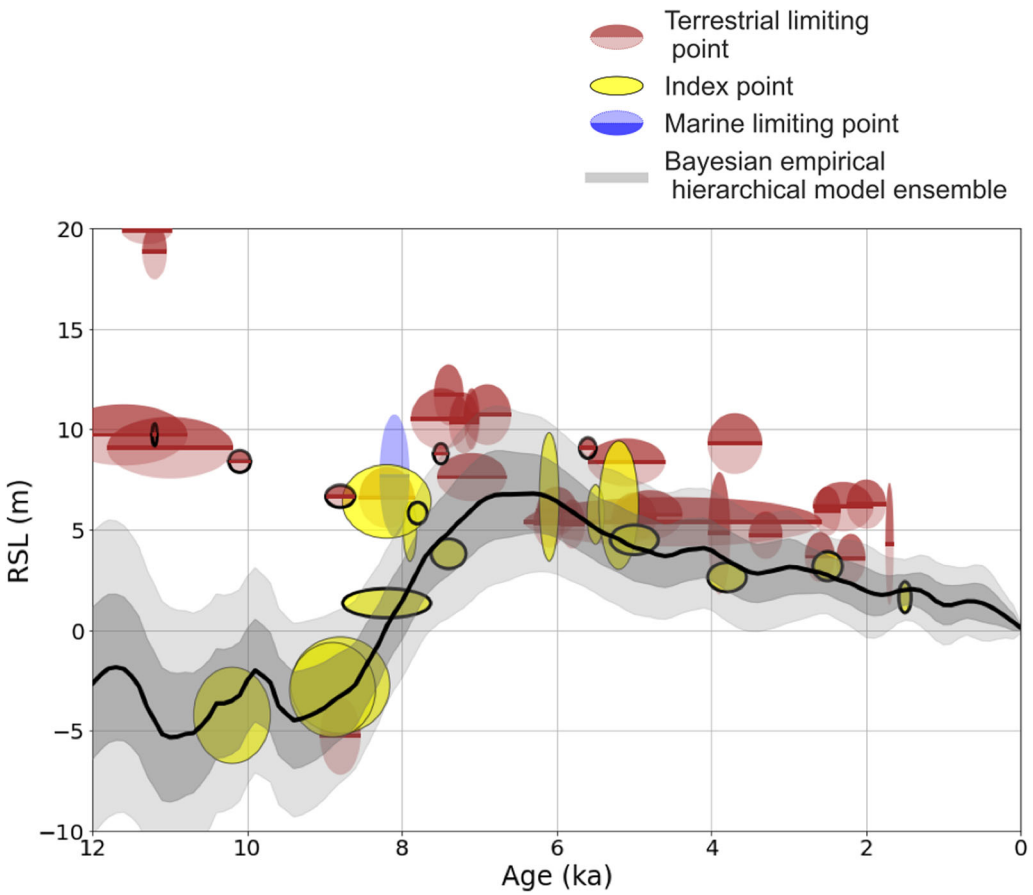


**Figure 11.** Holocene relative sea-level data and the spatio-temporal empirical hierarchical model ensemble (STEHME) predictions for Lofoten–Vesterålen. Data symbols correspond to the RSL indicator type with age and vertical uncertainties reported as 2σ (Table S1; Fig. S1) (Creel et al., 2022). Index points from this study have a black outline. The STEHME is shown in gray; the light gray band is the 95% confidence interval, the dark gray band is the 68% confidence interval and the black line is the mean.

recorded by isolation contacts in Storfjordvatnet, Farstadvatnet, Drågtjønna and Krystadvatnet (Figs. 3–7). Late Holocene RSL fall is also defined by data from an isolation basin (Balascio et al., 2011), coastal sequences (Marthinussen, 1962; Nydal et al., 1964; Møller, 1986) and archaeological sites (Utne, 1973; Møller, 1984; 1987). Salt marsh index points spanning the last 3.3k cal a BP at a site southeast of our study area in South Hinnøya (Barnett et al., 2015) were included in Creel et al. (2022). However, these data are all below c. 1.5 m above present levels and are anomalously low relative to other indicators in the region, possibly due to unaccounted-for salt marsh subsidence. Because of their proximity to the Lofoten–Vesterålen region, the index points from Barnett et al. (2015) influenced the STEHME to produce unrealistic late Holocene RSL trends around Lofoten. In particular, the STEHME from Creel et al. (2022) included RSL near Lofoten that reached present sea level c. 3k cal a BP, which is inconsistent with archaeological and other geomorphic evidence. These data from Barnett et al. (2015) were reassessed in our model as marine-limiting points.

Uncertainties in the STEHME are largest prior to c. 10k cal a BP and generally decrease up to the present day. The larger STEHME uncertainties in the early Holocene are due to the small number of index points prior to c. 10k cal a BP in comparison to the high number of index points that constrain the mid-Holocene transgression. Over the last c. 5k cal a BP there are fine-scale oscillations in the STEHME, which probably result from how the model optimizes to fit our late Holocene SLIPs. Given the model uncertainties during this interval, these oscillations are not significant.

The RSL history for Lofoten–Vesterålen defined by the STEHME updates the previous curve presented by Møller (1986) (Fig. 11). The general trends between the mean STEHME and the Møller (1986) curve are similar in that both show the same timing for the onset of the Tapes transgression and the Tapes maximum. The STEHME also updates the Møller (1986) curve by constraining RSL trends over the last 4k cal a BP based on our new SLIPs.

Additional details concerning the spatial pattern of RSL change for Lofoten–Vesterålen can be visualized using isobase maps generated from the STEHME (Fig. 12). Isobase lines depict contours of equivalent RSL change between the present day and a given time in the past. The 7k cal a BP isobases represent the differences in RSL elevations across the region between today and the Tapes transgression maximum. The shoreline gradient for this period is 0.25 m $km^{-1-}$ during the transgression maximum that ranges from c. 5 to 10 m from the outer to the inner islands of the archipelagos. Isobase maps for time intervals after the transgression maximum, at 5k and 3k cal a BP, show a progressive decrease in the regional shoreline gradient to 0.14 and 0.07 m $km^{-1-}$, respectively (Fig. 12). They also show the seaward motion of the zero isobase, which represents the 'hinge line' contour along which RSL is neither rising nor falling. This hinge-line migration, which proceeds at c. 7 km $ka^{-1-}$ between 7 and 3 ka, is comparable to rates of peripheral bulge migration documented along the eastern margin of the Laurentide Ice Sheet (Barnhardt et al., 1995), and is probably a function of the solid Earth structure beneath the region.

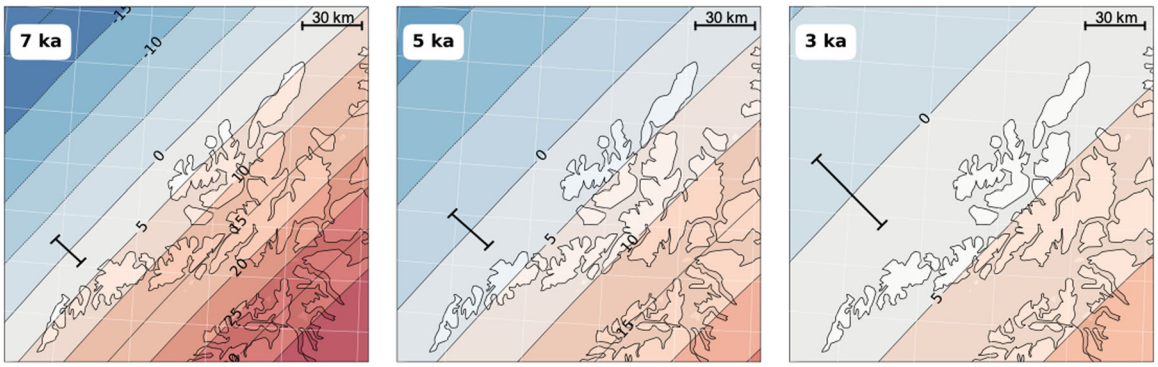


**Figure 12.** Isobase lines for Lofoten–Vesterålen based on the spatio-temporal empirical hierarchical model ensemble predictions. Contours (in meters) in panels from left to right represent relative sea level across the region at 7, 5 and 3k cal a BP. Approximate uncertainty ranges of isobase lines are represented as a black bar on the 0-m isobase for each time period.

## *Relationship between RSL and early human settlement of Lofoten–Vesterålen*

Holocene RSL variations have influenced the location and preservation of coastal settlement locations and harbors in Lofoten–Vesterålen from the Early Stone Age through historic intervals (Møller, 1987; Wickler, 2013; Balascio & Wickler, 2018). The earliest archaeological evidence for human presence in the region is documented in the Storbåthellaren rock shelter c. 8k cal a BP on the island of Flakstad in Lofoten (Utne, 1973). Initial human presence in Lofoten–Vesterålen was likely to have been significantly earlier, but potential settlement sites have been submerged or their preservation impacted by the Tapes transgression. The Storbåthellaren rock shelter site, located 7–8 m above MTL, provides terrestrial limiting data points that help define RSL fall following the Tapes transgression maximum and indicate the proximity of sea level to the site during initial human occupation (Fig. 11). Our knowledge of the Stone Age in both Lofoten and Vesterålen remains extremely limited, and although there is an abundance of site locations, only a handful have been archaeologically investigated. In Lofoten, these include a settlement site at Kolvika on Vestvågøy, partially excavated in 1969 and 1978 with Stone Age and Early Iron Age occupation (Jørgensen, 1989), and a Late Stone Age residential site dated to c. 5.6–5.3k cal a BP at Tjelbergvika on Austvågøy excavated by the Arctic University Museum of Norway in 2022 (Niemi, 2021). Many Stone Age sites with residential structures are in sheltered bays 10–20 m above current sea level that would have provided good harbor conditions when they were in use. Our refined RSL history for the region contributes to the improved understanding of sea-level positions during the Stone Age and the potential preservation or relative location of other sites throughout the region.

During the late Holocene, the relationship between human settlement and RSL is documented in the construction of boathouses. Following the onset of agriculture in the region c. 4.2k cal a BP, more substantial permanent settlements were established during the Iron Age (c. 2.5–0.9k cal a BP) and boathouse structures became important features of coastal communities (Wickler & Nilsen 2012). Boathouses were built along shorelines and therefore have an association with sea level at the time of construction (Wickler & Nilsen 2005, 2012). The island of Vestvågøy in Lofoten has the highest concentration of Iron Age boathouse remains in northern Norway with c. 62 dating to this period (Nilsen, 1998). Due to RSL lowering, the oldest boathouses are generally located higher than subsequent structures, although the relationship is complicated by the social context of boathouse construction and use, since they required significant time and resources to build and had a role in community structure (Wickler & Nilsen 2005; 2012). Nevertheless, they represent an important connection between human activity and past RSL elevations.

Boathouses were often constructed in embayments along the coast that provided protected natural harbors, which were also impacted by RSL lowering. The best example is Inner Borgpollen in Lofoten, which served as a harbor throughout the Iron Age and was associated with the prominent Viking Age chieftain settlement at Borg (Munch et al., 2003). Inner Borgpollen has narrow and shallow connections to the ocean today, and is salinity-stratified due to limited sea water input relative to freshwater derived from the watershed. It has been hypothesized that RSL lowering during the Iron Age, which was c. 2 m above present, made Inner Borgpollen less useful as a natural harbor because the connection to the ocean became restricted (Mills et al., 2009; Balascio and Wickler, 2018). Sea-level lowering would have: (i) made it more difficult for boats to navigate the channel into Inner Borgpollen and (ii) restricted the amount of seawater entering the basin, possibly leading to freezing of the surface water in winter, when the cod fisheries are most productive and harbor access would have been critical. Dates on cultural horizons identified in boathouses excavated around Inner Borgpollen, with dates ranging from the Roman Iron Age to early medieval period (c. 2–0.8k cal a BP), generally support this hypothesis (Wickler & Nilsen 2012).

The record from Inner Borgpollen we report here provides the most well-resolved history of salinity changes in the basin (Fig. 8). We identify the onset of brackish conditions to c. 1.5k cal a BP, which is at the end of the Early Iron Age and earlier than previously thought (Mills et al., 2009). This transition is associated with evidence for increased water column stratification and the start of a decline in surface water salinity. Although we cannot quantify salinity values and the potential for freezing in winter months, our data do indicate that changes in environmental conditions at Inner Borgpollen began at the start of the Late Iron Age and continued through the Viking Age (c. 1.5–0.9k cal a BP). These changes probably contributed to the eventual decline in the importance of the Inner Borgpollen as a harbor at the end of the Viking Age.

The impact of RSL change on the usefulness of harbors in the region continued into historic intervals. The natural harbor of Storvågan on the island of Austvågøy in Lofoten served the historic settlement of Vágar and played a critical role in the expansion of medieval settlement from c. 0.8 to 0.6k cal a BP. However, a gradual but steady decline in sea level made it increasingly difficult to access the harbor with deeper draft vessels that became more common in the late medieval period, contributing to the decline of the settlement (Wickler 2013: 64–65).

## Conclusions

This study presents new SLIPs for the Lofoten and Vesterålen archipelagos and combines them with previously published data to refine our understanding of the Holocene RSL history. SLIPs are based on interpretations of the stratigraphy of five isolation basins and one coastal sedimentary sequence. We show how sedimentary geochemical data, including carbon isotopes, scanning XRF and %S, can define detailed characteristics of marine, brackish and lacustrine phases of sedimentation in isolation basins. We compiled our new SLIPs with existing RSL data for the region using an STEHME. This approach better represents the spatial and temporal patterns in regional RSL trends by accounting for the vertical and temporal uncertainties in each index point and in the resulting RSL curve and isobase maps. Our revised RSL curve constrains the Tapes transgression from c. 9 to 6k cal a BP, associated with a sea level rise from −4 to 7 m above present day. Following the transgression, RSL fell rapidly from c. 6 to 5k cal a BP and then more gradually over the last 5k cal a BP. These trends generally follow the pattern of previous reconstructions, but provide additional constraints on the Tapes maximum and late Holocene RSL trends. Isobase maps generated from the STEHME for the last 7k cal a BP show the pattern of RSL change from inner and outer coastal environments of Lofoten and Vesterålen and quantify the progressive decrease in the regional RSL gradient. Our data also provide an improved understanding of the relationship between RSL and the local human history. RSL has impacted the location and preservation of coastal settlement locations and harbors in Lofoten and Vesterålen since the early Stone Age. We specifically investigated the timing of salinity changes in Inner Borgpollen, the Viking Age harbor associated with the chieftain settlement at Borg on Vestvågøya. Our data show that the onset of brackish conditions c. 1.5k cal a BP was during the Late Iron Age and probably influenced the decline in usefulness of the harbor supported by archaeological data. This example highlights RSL change as an important human–environment interaction for coastal Norway and in other coastlines influenced by significant Holocene RSL variations.

*Acknowledgements.* This work was funded by National Science Foundation (NSF) grants OPP-1504270 (N.L.B., W.J.D.), EAR-1660309 (N.L.B.) and EAR-2002352 (R.C.). Support was also provided by a U.S.–Norway Fulbright Scholar Award to N.L.B., a W&M Environment & Sustainability program Undergraduate Summer Research Fellowship to L.M., and a Charles Center Undergraduate Research Honors Fellowship to M.D. We thank Geir Are Johansen, Director of Museum Nord, and Marion Fjelde Larsen, Director of the Lofotr Viking Museum, for their support and assistance with field logistics. We also thank Martina Bixler, Eve Pugsley, Gabe Westergren and Lorelei Curtin for assistance in the field, and Isaac Mantelli, Sarah Snipes, Nicholas Montalbano and Rebecca Topness for assistance in the laboratory.

### *Data availability statement*

The data that support the findings of this study are available at Zenodo.com, an open science and open data repository. Datasets include sediment geochemical data (https://doi.org/10.5281/zenodo.8421400) as well as model data and outputs (https://doi.org/10.5281/zenodo.10476054).

## Supporting information

Additional supporting information may be found in the online version of this article at the publisher's web-site.

**Figure S1.** Presenting the timeseries of sea-level index points, terrestrial limiting, and marine limiting points with all data points labelled and referenced to Table S1.

**Table S1.** Presenting all sea-level index points, terrestrial limiting, and marine limiting data points for Lofoten and Vesterålen represented in Figure 11.

*Abbreviations.* DGPS, differential global positioning system; FIS, Fennoscandian Ice Sheet; GMSL, global mean sea level; GPS, global positioning system; MHWNT, mean high water neap tide; MHWST, mean high water spring tide; MLWST, mean low water spring tide; MS, magnetic susceptibility; MSL, mean sea level; RMSE, root mean squared error; RSL, relative sea level; SLIP, sea-level index point; STEHME, spatiotemporal empirical hierarchical ensemble; TC, total carbon; XRF, X-ray florescence.

## References

Balascio, N.L. & Wickler, S. (2018) Human-environment dynamics during the Iron Age in the Lofoten Islands. *Norsk Geografisk Tidsskrift - Norwegian Journal of Geography*, 72, 146–160.

Balascio, N.L., Zhang, Z., Bradley, R.S., Perren, B., Dahl, S.O. & Bakke, J. (2011) A multi-proxy approach to assessing isolation basin stratigraphy from the Lofoten Islands, Norway. *Quaternary Research*, 75, 288–300.

Baranskaya, A.V., Khan, N.S., Romanenko, F.A., Roy, K., Peltier, W.R. & Horton, B.P. (2018) A postglacial relative sea-level database for the Russian Arctic coast. *Quaternary Science Reviews*, 199, 188–205.

Barnett, R.L., Gehrels, W.R., Charman, D.J., Saher, M.H. & Marshall, W.A. (2015) Late Holocene sea-level change in arctic Norway. *Quaternary Science Reviews*, 107, 214–230.

Barnhardt, W.A., Belknap, D.F. & Kelley, J.T. (1997) Stratigraphic evolution of the inner continental shelf in response to late Quaternary relative sea-level change, northwestern Gulf of Maine. *Geological Society of America bulletin*, 109, 612–630.

Barnhardt, W.A., Roland Gehrels, W. & Kelley, J.T. (1995) Late Quaternary relative sea-level change in the western Gulf of Maine: evidence for a migrating glacial forebulge. *Geology*, 23, 317–320.

Blaauw, M. & Christen, J.A. (2011) Flexible paleoclimate age-depth models using an autoregressive gamma process. *Bayesian Analysis*, 6, 457–474.

Bondevik, S., Stormo, S.K. & Skjerdal, G. (2012) Green mosses date the Storegga tsunami to the chilliest decades of the 8.2 ka cold event. *Quaternary Science Reviews*, 45, 1–6.

Bondevik, S., Svendsen, J.I., Johnsen, G., Mangerud, J. & Kaland, P.E. (1997a) The Storegga tsunami along the Norwegian coast, its age and run up. *Boreas*, 26, 29–53.

Bondevik, S., Svendsen, J.I. & Mangerud, J. (1997b) Tsunami sedimentary facies deposited by the Storegga tsunami in shallow marine basins and coastal lakes, western Norway. *Sedimentology*, 44, 1115–1131.

Boutton, T.W. (1991) Stable carbon isotope ratios of natural materials: II. Atmospheric, terrestrial, marine, and freshwater environment. *In*: Coleman, D.C. & Fry, B., (eds) *rbon Isotope Techniques*. London: Academic Press. pp. 173–185.

Brendryen, J., Haflidason, H., Yokoyama, Y., Haaga, K.A. & Hannisdal, B. (2020) Eurasian Ice Sheet collapse was a major source of Meltwater Pulse 1 A 14,600 years ago. *Nature Geoscience*, 13, 363–368.

Corner, G.D. & Haugane, E. (1993) Marine-lacustrine stratigraphy of raised coastal basins and postglacial sea-level change at Lyngen and Vanna, Troms, northern Norway. *Norsk Geologisk Tidsskrift*, 73, 175–197.

Corner, G.D., Yevzerov, V.Y., Kolka, V.V. & Møller, J.J. (1999) Isolation basin stratigraphy and Holocene relative sea-level change at the Norwegian-Russian border north of Nikel, northwest Russia. *Boreas*, 28, 146–166.

Cornwell, J.C. & Morse, J.W. (1987) The characterization of iron sulfide minerals in anoxic marine sediments. *Marine Chemistry*, 22, 193–206.

Creel, R.C., Austermann, J., Khan, N.S., D'Andrea, W.J., Balascio, N., Dyer, B. et al. (2022) Postglacial relative sea level change in Norway. *Quaternary Science Reviews*, 282, 107422.

Croudace, I.W., Rindby, A. & Rothwell, R.G. (2006) ITRAX: description and evaluation of a new multi-function X-ray core scanner. *In*: Rothwell, R.G. (Ed.), New Techniques in Sediment Core Analysis, 267. Geological Society, London, Special Publications, pp. 51–564.

Ding, X., Li, D., Zheng, L., Bao, H., Chen, H.-F. & Kao, S.J. (2016) Sulfur geochemistry of a lacustrine record from Taiwan reveals enhanced marine aerosol input during the early Holocene. *Scientific Reports*, 6, 38989.

Fjeldskaar, W. (1994) The amplitude and decay of the glacial forebulge in Fennoscandia. *Norsk Geologisk Tidsskrift*, 74, 2–8.

Fjeldskaar, W. & Bondevik, S. (2020) The Early-Mid Holocene transgression (Tapes) at the Norwegian coast – comparing observations with numerical modelling. *Quaternary Science Reviews*, 242, 106435.

Fogel, M., Cifuentes, L., Velinsky, D. & Sharp, J. (1992) Relationship of carbon availability in estuanne phytoplankton to isotopic composition. *Marine Ecology Progress Series*, 82, 291–300.

Fogel, M.L. & Cifuentes, L.A. (1993) Isotope fractionation during primary production. *In*: Engel, M.H. & Macko, S.A., (eds) *Organic Geochemistry, Topics in Geobiology*. New York: Springer. pp. 73–98.

Fægri, K. (1944) On the introduction of agriculture in western Norway. *Geologiska Föreningen i Stockholm Förhandlingar*, 66, 449–462.

Fægri, K. & Iversen, J. (1989) *Textbook of Pollen Analysis*. Chichester: Wiley.

Glørstad, H. (2015) Deglaciation, sea-level change and the Holocene colonization of Norway. *Geological Society, London, Special Publications*, 411, 9–25.

Helskog, K. (1978) Late Holocene sea-level changes seen from prehistoric settlements. *Norsk Geografisk Tidsskrift - Norwegian Journal of Geography*, 32, 111–119.

Holmboe, J. (1903) Planterester i norske torvmyrer. Vidensk.-Selsk. Skr., Math.-Na turv. Kl., No. 2 (Kristiania).

Holmer, M. & Storkholm, P. (2001) Sulphate reduction and sulphur cycling in lake sediments: a review. *Freshwater Biology*, 46, 431–451.

Jankovská, V. & Komárek, J. (2000) Indicative value of Pediastrum and other coccal green algae in palaeoecology. *Folia Geobotanica*, 35, 59–82.

Jessen, C.A., Rundgren, M., Björck, S., Andresen, C.S. & Conley, D.J. (2008) Variability and seasonality of North Atlantic climate during the early Holocene: evidence from Faroe Island lake sediments. *The Holocene*, 18, 851–860.

Jørgensen, R. (1989) En boplasstype fra eldre metallalder i Nordland. *In*: Bertelsen, R., Reymert, P. K. & Utne, A. (eds.) Framskritt for fortida i nord: i Povl Simonsens fotefar, 135-145. Tromsø Museums Skrifter XXII. Tromsø Museum: Tromsø.

Kaland, P.E. (1984) Holocene shore displacement and shorelines in Hordaland, western Norway. *Boreas*, 13, 203–242.

Kartverket (2021) Tide Tables for the Norwegian Coast and Svalbard. The Norwegian Mapping Authority: Stavanger.

Kjemperud, A. (1981) Diatom changes in sediments of basins possessing marine/lacustrine transitions in Frosta, Nord-Trøndelag, Norway. *Boreas*, 10, 27–38.

Komárek, J. & Jankovská, V. (2001) Review of the green algal genus Pediastrum; implication for pollen-analytical research. J Cramer: Berlin.

Lamb, A.L., Wilson, G.P. & Leng, M.J. (2006) A review of coastal palaeoclimate and relative sea-level reconstructions using δ13C and C/N ratios in organic material. *Earth-Science Reviews*, 75, 29–57.

Lambeck, K., Smither, C. & Johnston, P. (1998) Sea-level change, glacial rebound and mantle viscosity for northern Europe. *Geophysical Journal International*, 134, 102–144.

Leng, M.J., Wagner, B., Anderson, N.J., Bennike, O., Woodley, E. & Kemp, S.J. (2012) Deglaciation and catchment ontogeny in coastal south-west Greenland: implications for terrestrial and aquatic carbon cycling. *Journal of Quaternary Science*, 27, 575–584.

Leri, A.C., Hakala, J.A., Marcus, M.A., Lanzirotti, A., Reddy, C.M. & Myneni, S.C.B. (2010) Natural organobromine in marine sediments: New evidence of biogeochemical Br cycling. *Global Biogeochemical Cycles*, 24, GB4017.

Lohne, Ø.S., Bondevik, S., Mangerud, J. & Svendsen, J.I. (2007) Sea-level fluctuations imply that the Younger Dryas ice-sheet expansion in western Norway commenced during the Allerød. *Quaternary Science Reviews*, 26, 2128–2151.

Mackie, E.A.V., Leng, M.J., Lloyd, J.M., & Arrowsmith, C. (2005) Bulk organic δ 13C and C/N ratios as palaeosalinity indicators within a Scottish isolation basin. *Journal of Quaternary Science*, 20, 303–312.

Mackie, E.A.V., Lloyd, J.M., Leng, M.J., Bentley, M.J., & Arrowsmith, C. (2007) Assessment of δ 13C and C/N ratios in bulk organic matter as palaeosalinity indicators in Holocene and Lateglacial isolation basin sediments, northwest Scotland. *Journal of Quaternary Science*, 22, 579–591.

Marthinussen, M. (1962) 14C-datings referring to shore lines, transgressions, and glacial substages in Northern Norway. *Norges geologiske undersøkelse*, 215, 37–67.

Mayer, L.M., Macko, S.A., Mook, W.H. & Murray, S. (1981) The distribution of bromine in coastal sediments and its use as a source indicator for organic matter. *Organic Geochemistry*, 3, 37–42.

Mayer, L.M., Schick, L.L., Allison, M.A., Ruttenberg, K.C. & Bentley, S.J. (2007) Marine vs. terrigenous organic matter in Louisiana coastal sediments: the uses of bromine:organic carbon ratios. *Marine Chemistry*, 107, 244–254.

Meyers, P.A. (1994) Preservation of source identification of sedimentary organic matter during and after deposition. *Chemical Geology*, 144, 289–302.

Meyers, P.A. (2003) Applications of organic geochemistry to paleolimnological reconstructions: a summary of examples from the Laurentian Great Lakes. *Organic Geochemistry*, 34, 261–289.

Midtun, E.S. (2019) Holosen Strandforskyvning for Leknes, Vestvågøy. Master's thesis. University of Bergen.

Mills, K., Mackay, A.W., Bradley, R.S. & Finney, B. (2009) Diatom and stable isotope records of late-Holocene lake ontogeny at Indrepollen, Lofoten, NW Norway: a response to glacio-isostasy and Neoglacial cooling. *The Holocene*, 19, 261–271.

Mitchell, M.J., Schindler, S.C., Owen, J.S. & Norton, S.A. (1988) Comparison of sulfur concentrations within lake sediment profiles. *Hydrobiologia*, 157, 219–229.

Munch, G.S., Johansen, O.S. & Roesdahl, E. (eds.) (2003) Borg in Lofoten: a Chieftain's Farm in North Norway. Lofotr Arkeologisk Skriftserie 1. Trondheim: Tapir Academic Press.

Møller, J.J. (1984) Holocene shore displacement at Nappstraumen, Lofoten, north Norway. *Norsk Geologisk Tidsskrift*, 64, 1–5.

Møller, J.J. (1985) Coastal caves and their relation to early postglacial shore levels in Lofoten and Vesterålen. *North Norway. Norsk Geologisk Undersøkelse*, 400, 51–65.

Møller, J.J. (1986) Holocene transgression maximum about 6000 years bp at Ramså, Vesterålen, north Norway. *Norsk Geografisk Tidsskrift - Norwegian Journal of Geography*, 40, 77–84.

Møller, J.J. (1987) Shoreline relation and prehistoric settlement in northern Norway. *Norsk Geografisk Tidsskrift - Norwegian Journal of Geography*, 41, 45–60.

Møller, J.J. (1989) Geometric simulations and mapping of Holocene relative sea-level changes in northern Norway. *Journal of Coastal Research*, 5, 403–417.

Niemi, A.R. (2021) Prosjektplan for Tjeldbergvika, Vågan kommune, Nordland fylke. Boplasser fra steinalder, Id. 214106 og 214109. Tromsø: Arctic University Museum of Norway.

Nilsen, G. (1998) Jernaldernaust på Vestvågøy i Lofoten. Master's thesis. Tromsø: University of Tromsø.

Nydal, R. (1962) Trondheim natural radiocarbon measurements III. *Radiocarbon*, 4, 160–182.

Nydal, R., Gulliksen, S. & Lövseth, K. (1972) Trondheim natural radiocarbon measurements VI. *Radiocarbon*, 14, 418–451.

Nydal, R., Lövseth, K., Skullerud, K.E. & Holm, M. (1964) Trondheim natural radiocarbon measurements IV. *Radiocarbon*, 6, 280–290.

Orme, L.C., Davies, S.J. & Duller, G.A.T. (2015) Reconstructed centennial variability of Late Holocene storminess from Cors Fochno, Wales, UK. *Journal of Quaternary Science*, 30, 478–488.

Patton, H., Hubbard, A., Andreassen, K., Auriac, A., Whitehouse, P.L., Stroeven, A.P. et al. (2017) Deglaciation of the Eurasian ice sheet complex. *Quaternary Science Reviews*, 169, 148–172.

Reimer, P.J., Austin, W.E.N., Bard, E., Bayliss, A., Blackwell, P.G., Bronk Ramsey, C. et al. (2020) The IntCal20 Northern Hemisphere Radiocarbon Age Calibration Curve (0–55 cal kBP). *Radiocarbon*, 62, 725–757.

Romundset, A. & Bondevik, S. (2011) Propagation of the Storegga tsunami into ice-free lakes along the southern shores of the Barents Sea. *Journal of Quaternary Science*, 26, 457–462.

Romundset, A., Bondevik, S. & Bennike, O. (2011) Postglacial uplift and relative sea level changes in Finnmark, northern Norway. *Quaternary Science Reviews*, 30, 2398–2421.

 

Romundset, A., Fredin, O. & Høgaas, F. (2015) A Holocene sea-level curve and revised isobase map based on isolation basins from near the southern tip of Norway. *Boreas*, 44, 383–400.

Romundset, A., Lakeman, T.R. & Høgaas, F. (2018) Quantifying variable rates of post-glacial relative sea level fall from a cluster of 24 isolation basins in southern Norway. *Quaternary Science Reviews*, 197, 175–192.

Romundset, A., Lohne, Ø.S., Mangerud, J. & Svendsen, J.I. (2010) The first Holocene relative sea-level curve from the middle part of Hardangerfjorden, western Norway. *Boreas*, 39, 87–104.

Rothwell, R.G., Hoogakker, B., Thomson, J., Croudace, I.W. & Frenz, M. (2006) Turbidite emplacement on the southern Balearic abyssal Plain (western Mediterranean Sea) during Marine isotope stages 1–3: an application of ITRAX XRF scanning of sediment cores to lithostratigraphic analysis. *In*: Rothwell, R.G., (Ed.) *New Techniques in Sediment core Analysis. Special Publications*. London: Geological Society. pp. 79–98.

Schofield, J.E., Edwards, K.J., Mighall, T.M., Martínez Cortizas, A., Rodríguez-Racedo, J. & Cook, G. (2010) An integrated geochemical and palynological study of human impacts, soil erosion and storminess from southern Greenland since c. AD 1000. *Palaeogeography, Palaeoclimatology, Palaeoecology*, 295, 19–30.

Shennan, I. & Horton, B. (2002) Holocene land- and sea-level changes in Great Britain. *Journal of Quaternary Science*, 17, 511–526.

Shennan, I., Horton, B., Innes, J., Gehrels, R., Lloyd, J., McArthur, J. et al. (2000) Late Quaternary sea-level changes, crustal movements and coastal evolution in Northumberland, UK. *Journal of Quaternary Science*, 15, 215–237.

Shennan, I., Long, A.J. & Horton, B.P. (2015) *Handbook of Sea-Level Research*. John Wiley & Sons.

Simms, A.R., Best, L., Shennan, I., Bradley, S.L., Small, D., Bustamante, E. et al. (2022) Investigating the roles of relative sea-level change and glacio-isostatic adjustment on the retreat of a marine based ice stream in NW Scotland. *Quaternary Science Reviews*, 277, 107366.

Simpson, M.J.R., Breili, K. & Kierulf, H.P. (2014) Estimates of twenty-first century sea-level changes for Norway. *Climate Dynamics*, 42, 1405–1424.

Sparrenbom, C.J., Bennike, O., Björck, S. & Lambeck, K. (2006) Relative sea-level changes since 15 000 cal. yr BP in the Nanortalik area, southern Greenland. *Journal of Quaternary Science*, 21, 29–48.

Steffen, H. & Wu, P. (2011) Glacial isostatic adjustment in Fennoscandia—A review of data and modeling. *Journal of Geodynamics*, 52, 169–204.

Stewart, H., Bradwell, T., Bullard, J., Davies, S.J., Golledge, N. & Mcculloch, R.D. (2017) 8000 years of North Atlantic storminess reconstructed from a Scottish peat record: implications for Holocene atmospheric circulation patterns in Western Europe. *Journal of Quaternary Science*, 32, 1075–1084.

Strunk, A., Larsen, N.K., Nilsson, A., Seidenkrantz, M.-S., Levy, L.B., Olsen, J. et al. (2018) Relative sea-level changes and ice sheet history in Finderup Land, north Greenland. *Frontiers in Earth Science*, 6, 129.

Stuiver, M., Reimer, P.J. & Reimer, R.W., 2020, CALIB 8.2 [WWW program] at http://calib.org

Svendsen, J.I. & Mangerud, J. (1987) Late Weichselian and holocene sea-level history for a cross-section of western Norway. *Journal of Quaternary Science*, 2, 113–132.

Svendsen, J.I. & Mangerud, J. (1990) Sea-level changes and pollen stratigraphy on the outer coast of Sunnmøre, western Norway. *Norsk Geologisk Tidsskrift*, 70, 111–134.

Turner, T.E., Swindles, G.T. & Roucoux, K.H. (2014) Late Holocene ecohydrological and carbon dynamics of a UK raised bog: impact of human activity and climate change. *Quaternary Science Reviews*, 84, 65–85.

Utne, A. (1973) En veidekulturs-boplass i Lofoten: Storbåthallaren ved Nappstraumen. Master's thesis. Tromsø: University of Tromsø.

Vasskog, K., Svendsen, J.-I., Mangerud, J., Agasøster Haaga, K., Svean, A. & Lunnan, E.M. (2019) Evidence of early deglaciation (18000 cal a bp) and a postglacial relative sea- level curve from southern Karmøy, south-west Norway. *Journal of Quaternary Science*, 34, 410–423.

Vetti, R.K.S. (2020) Isavsmelting Og Postglasiale Havnivåendringer Ved Nykvåg, Vesterålen. Master's Thesis. The University of Bergen.

Vorren, K.-D. (1978) Late and Middle Weichselian stratigraphy of Andøya, north Norway. *Boreas*, 7, 19–38.

Vorren, K.-D. & Moe, D. (1986) The early Holocene climate and sea-level changes in Lofoten and Vesterålen, North Norway. *Norsk Geologisk Tidsskrift*, 66, 135–143.

Vorren, T.O., Vorren, K.-D., Alm, T., Gulliksen, S. & Løvlie, R. (1988) The last deglaciation (20,000 to 11,000 B. P.) on Andoya, northern Norway. *Boreas*, 17, 41–77.

Westman, P. & Hedenström, A. (2002) Environmental changes during isolation processes from the Litorina Sea as reflected by diatoms and geochemical parameters – a case study. *The Holocene*, 12, 531–540.

Whitehouse, P.L., Gomez, N., King, M.A. & Wiens, D.A. (2019) Solid Earth change and the evolution of the Antarctic Ice Sheet. *Nature Communications*, 10, 503.

Wickler, S. (2013) The potential of shoreline and shallow submerged Iron Age and medieval archaeological sites in the Lofoten Islands, northern Norway. *In* Daire, M.-Y., Dupont, C., Baudry, A., Billard, C., Large, J.-M., Lespez, L., Normand, E. & Scarre, C. (eds.) Ancient Maritime Communities and the Relationship Between People and Environment along the European Atlantic Coasts, 63–74. British Archaeological Reports International Series 2570. Oxford: Archaeopress.

Wickler, S. & Nilsen, G. (2012) Pre-modern boathouses: a maritime perspective from northern Norway. *International Journal of Nautical Archaeology*, 41, 106–119.

Wickler, S. & Nilsen, G. (2005) Iron Age boathouses in Arctic Norway viewed as multifunctional expressions of maritime cultural heritage. *In*: Marcet, I., Barbe, R., Brebbia, C.A. & Olivella, J., (eds.) *Maritime Heritage and Modern Ports*. Southhampton: WIT Press. pp. 15–23

Ziegler, M., Jilbert, T., de Lange, G.J., Lourens, L.J. & Reichart, G.-J. (2008) Bromine counts from XRF scanning as an estimate of the marine organic carbon content of sediment cores. *Geochemistry, Geophysics, Geosystems*, 9, Q05009.